THE EFFECT OF BONE SURFACE MIMICKED MAGNETIC PARTICLE EMBEDDED PDMS MEMBRANES ON HUMAN OSTEOBLAST BEHAVIOR

by

Berkay Erenay

B.S., in Bioengineering, Istanbul Technical University & Montana State University, 2015

Submitted to the Institute of Biomedical Engineering
in partial fulfillment of the requirements
for the degree of
Master of Science
in
Biomedical Engineering

Boğaziçi University
2019

THE EFFECT OF BONE SURFACE MIMICKED MAGNETIC PARTICLE EMBEDDED PDMS MEMBRANES ON HUMAN OSTEOBLAST BEHAVIOR

APPROVED BY:

Assoc. Prof. Dr. Bora Garipcan .....
(Thesis Advisor)

Assoc. Prof. Dr. Sedat Odabaş .....
(Thesis Co-advisor)

Assoc. Prof. Dr. Esin Öztürk Işık .....

Assist. Prof. Dr. Duygu Ege .....

Prof. Dr. Kadriye Tuzlakoğlu .....

DATE OF APPROVAL: 26 July 2019

ACKNOWLEDGMENTS

I want to express my deepest gratitude and appreciation to dearest Assoc. Prof. Dr. Bora Garipcan and Assoc Prof. Dr. Sedat Odabaş for their wisdom, knowledge, guidance and help, both in academia and in life across all these years. I couldn't ask for better advisors.

I thank my family for their unwavering support and unconditional love. They entrusted me their hopes and dreams and always wanted me to be the best I can. There is no way for me to pay them back what they have done for me all these years.

I want to thank my dear colleagues and friends in Bioscubus Research Laboratory for all their support in every area imaginable and for all their academic input and insight during my work. I exclusively want to thank Alp Özgün and Özgen Öztürk for all their selflessness whenever I needed support. They have taught, mentored and helped me all these years. I also especially thank Burak Altun and Melis Toker for sharing the same stress and for all their wholehearted friendship. We were on the same boat during our time here and we have sailed this vast sea together. I really wish all these years to come would strengthen the bond that we have forged during our journey.

This study was financially supported by TÜBİTAK with Project Grant Number: 217M551 and Boğaziçi University Research Fund Grant Number: 6701.

I dedicate this thesis to the loving memory of my grandparents who taught me to learn from my mistakes, being kind, polite, resilient and diligent. They have always encouraged me to keep trying in every aspect of life and continue to move forward.

I will always keep moving forward.

ACADEMIC ETHICS AND INTEGRITY STATEMENT

I, Berkay Erenay, hereby certify that I am aware of the Academic Ethics and Integrity Policy issued by the Council of Higher Education (YÖK) and I fully acknowledge all the consequences due to its violation by plagiarism or any other way.

Name :

Signature:

Date:

ABSTRACT

THE EFFECT OF BONE SURFACE MIMICKED MAGNETIC PARTICLE EMBEDDED PDMS MEMBRANES ON HUMAN OSTEOBLAST BEHAVIOR

Cell microenvironment can be defined as all biophysical, biochemical, biomechanical properties that affect cell behaviour and cell fate. These factors include surface topography, roughness, stiffness along with the extracellular matrix (ECM) and presence of other soluble factors. Changes in the microenvironment are directly or indirectly converted into signalling pathways inside the cell and affect cellular metabolism. In this thesis, effects of surface topography and surface chemistry were investigated by synthesizing magnetic particle embedded (MP) (0.5% w/w) bone surface mimicked (BSM) polydimetylsiloxane (PDMS) membranes on osteoblast behavior. Bone tissue microenvironment were imitated by chemically modifying membrane surfaces with extracellular matrix proteins Fibronectin and Collagen-I. Human fetal osteoblast cells (hFOB) were seeded on these magnetic particle embedded bone surface mimicked scaffolds in order to observe potential differences in osteoblast behavior. Material characterization for all membranes were done using Water Contact Angle (WCA) measurements, Vibrating Sample Magnetometry (VSM), Fourier Transform Infrared Spectroscopy (FTIR), Scanning Electron Microscopy (SEM), and Transmission Electron Microscopy (TEM). Cellular behaviour on these membranes were investigated using alamarBlue cell proliferation assay, indirect MTT assay, actin and nuclear fluorescent stainings. Results of these study indicated that the protein modifications and surface topography resulted from bone surface pattern transfer to membrane surfaces have increased osteoblast adhesion and proliferation. Cell morphologies were natural and consistent with previous findings but further experimentations are required to understand possible effects of embedded magnetic particles (Fe_3O_4) on mechanotransductive and intracellular signalling pathways.

Keywords: PDMS, Bone Surface Mimicking, Magnetic Particle, Protein Modification.

ÖZET

MANYETİK PARTİKÜL İÇEREN KEMİK YÜZEY TAKLİTLİ PDMS MEMBRANLARIN İNSAN OSTEOBLAST HÜCRESİ DAVRANIŞLARINA ETKİSİ

Hücre mikroçevresi, hücre davranışlarına ve hücre metabolizmasına etki eden biyofiziksel, biyokimyasal ve biyomekanik özelliklerin tümü olarak tanımlanabilir. Bu özellikler, yüzeylerin topografyası, pürüzlülüğü ve sertliğinin yanı sıra hücre dışı matris ve çeşitli çözülebilir faktörleri içermektedir. Hücre mikroçevresi üzerindeki değişiklikler doğrudan ya da dolaylı olarak hücre içerisindeki çeşitli sinyal yolağlarını aktifleştirerek hücre metabolizmasını etkilemektedir. Bu tezde, manyetik partikül gömülü (ağırlığınca %0.5) kemik yüzey taklitli polidimetilsiloksan yüzeylerin hücre metabolizması ve davranışları üzerindeki etkileri incelenmiştir. Kemik dokusu mikroçevresi, kemik yüzey taklitli membran yüzeylerinin hücre dışı matris proteinleri olan Fibronektin ve Kollajen-I ile kimyasal olarak modifiye edilmesi ile taklit edilmiştir. Hücre metabolizması üzerindeki olası etkilerin gözlemlenmesi için insan osteoblast hücreleri bu manyetik partikül gömülü kemik yüzey taklitli membranların üzerine ekilmiştir. PDMS membranların malzeme karakterizasyonları için su temas açısı, Titreşimli Örnek Manyetometresi, Fourier transform kızılötesi spektrometresi, Taramalı Elektron Mikroskobu ve Transmisyon Elektron Mikroskobu kullanılmıştır. Hücre davranışlarının gözlemlenmesi için alamarBlue hücre proliferasyon tayini, indirekt MTT sitotoksisite tayini ve aktin hücre iskeleti ve çekirdek boyamaları gerçekleştirilmiştir. Çalışma sonuçları göstermektedir ki, protein modifikasyonu ve kemik yüzey dokusunun membran yüzeylerine transferinden kaynaklı artış gösteren pürüzlülük, osteoblast hücre tutunması ve proliferasyonu arttırmıştır. Hücre morfolojilerinin doğal olduğu gözlemlenmiş ancak manyetik partiküllerin mekanotransdüktif ve hücre içi sinyal yolağları üzerinde olası etkilerinin gözlemlenmesi için daha fazla çalışma yapılması gerekmektedir.

Anahtar Sözcükler: PDMS, Kemik Yüzey Taklidi, Manyetik Partikül, Protein Modifikasyonu.

TABLE OF CONTENTS

ACKNOWLEDGMENTS . . . iii
ACADEMIC ETHICS AND INTEGRITY STATEMENT . . . iv
ABSTRACT . . . v
ÖZET . . . vi
LIST OF FIGURES . . . ix
LIST OF TABLES . . . xii
LIST OF SYMBOLS . . . xiii
LIST OF ABBREVIATIONS . . . xiv
1. INTRODUCTION . . . 1
1.1 Motivation . . . 1
1.2 Objective . . . 3
1.3 Outline . . . 4
2. BACKGROUND . . . 5
2.1 Bone structure . . . 5
2.2 Biology of Bone . . . 8
2.3 Cellular Microenvironment . . . 9
2.4 Biomaterials used in Bone Regeneration Applications . . . 10
2.5 Properties of Polydimethylsiloxane (PDMS) . . . 11
2.6 Effects of magnetism on cell metabolism . . . 12
3. MATERIALS AND METHODS . . . 14
3.1 Bone Xenograft Cleaning . . . 14
3.2 Magnetic particle synthesis . . . 15
3.3 Production of PDMS Membranes . . . 16
3.3.1 Preperation of plain PDMS membranes . . . 16
3.3.2 Preperation of Bone surface mimicked PDMS membranes (BSM PDMS) . . . 16
3.4 Protein Modification . . . 18
3.5 Material Characterization . . . 18
3.5.1 Water Contact Angle Measurements (WCA) . . . 18

3.5.2 Transmission Electron Microscopy (TEM) 19
3.5.3 Vibrating Sample Magnetometer (VSM) 19
3.5.4 Investigation of Membrane Topographies 19
3.5.5 Atomic Force Microscopy (AFM) 19
3.5.6 Fourier Transform Infrared Spectroscopy (FTIR) 20
3.6 Cell culture studies 20
3.6.1 Indirect MTT Cytotoxicity assay 20
3.6.2 alamarBlue cell proliferation assay 21
3.6.3 Flourescent Imaging 21
4. RESULTS 22
4.1 Material Characterization 22
4.1.1 Magnetization Measurements 22
4.1.2 Water Contact Angle Measurements 23
4.1.3 Atomic Force Microscopy (AFM) 24
4.1.4 Transmission Electron Microscopy (TEM) 25
4.1.5 Investigation of Membrane Topograpies 26
4.1.6 Fourier Transform Infrared Spectroscopy (FTIR) 27
4.2 Cell Culture Studies 29
4.2.1 Indirect MTT cytotoxicity assay 29
4.2.2 Elimination studies 29
4.2.3 alamarBlue Cell proliferation assay 33
4.2.4 Fluorescent Imaging 35
4.3 Statistical Analysis 41
5. DISCUSSION 42
5.1 Material Characterization 42
5.2 Cell culture studies 45
5.3 Conclusion 51
5.4 Future studies 52
APPENDIX A. SUPPLEMENTARY INFORMATION 53
A.1 Bradford Protein Quantification Assay 53
REFERENCES 55

LIST OF FIGURES

Figure 2.1	Layers of periosteum.	7
Figure 2.2	Macroscopic anatomy of bone.	7
Figure 2.3	Osteogenic pathways of mesenchymal stem cell differentiation.	9
Figure 3.1	Schematic of xenograft bone cleaning process.	14
Figure 3.2	Schematic of magnetic particle synthesis.	15
Figure 3.3	Preperation of BSM PDMS membranes.	17
Figure 3.4	PDMS membranes with different concentrations of magnetic particles embedded. (A) Plain PDMS, (B) 0.5% mpPDMS, (C) 1% mpPDMS, (D) 2% mpPDMS.	17
Figure 3.5	PDMS membranes with different approaches of bone surface mimicry. (A) Plain PDMS, (B)BSM PDMS,(C)BSM PDMS (before optimization).	18
Figure 4.1	Magnetization measurements of PDMS membranes with different magnetic particle concentrations.	22
Figure 4.2	Water contact angle images of PDMS membranes with different topography and protein modifications (A) Plain PDMS, (B) 0.5% mpPDMS, (C) 1% mpPDMS, (D) BSM PDMS, (E) 0.5% BSM mpPDMS, (F) 1% BSM mpPDMS, (G) Plain PDMS+Col-I, (I) Plain PDMS+FN, (J) Negative BSM PDMS, (L) BSM PDMS+Col-I, (M) BSM PDMS+FN.	23
Figure 4.3	AFM surface profile for different PDMS membranes. (A) Surface profile for Plain PDMS membrane, (B) Surface profile for BSM PDMS membrane.	24
Figure 4.4	TEM image of synthesized magnetic particles (Scale bar: 20nm).	25
Figure 4.5	Histogram of the TEM image of magnetic nanoparticles, showing the number of particles counted in different size ranges. Average particle size and standard deviation is given on the graph.	26

Figure 4.6 Comparison of surface topographies of bovine femur bone, BSM PDMS membranes and plain PDMS membranes. (A) Bovine Femur Bone, (B) BSM PDMS membrane. (C),(D) Plain PDMS membranes (2500x), (E) BSM PDMS membrane (100x), (F) BSM PDMS membrane (2500x). 27

Figure 4.7 FTIR Spectra of plain PDMS, 0.5% mpPDMS and 1% mpPDMS membranes. Characteristic Fe-O bands were enlarged for visibility. 28

Figure 4.8 FTIR Spectra of PDMS, PDMS+FN and PDMS+Col-I membranes. Secondary amine band around 3345 cm^{-1}. Protein specific bands were enlarged for visibility. 28

Figure 4.9 Indirect MTT cytotoxicity assay. 29

Figure 4.10 alamarBlue cell proliferation assay to assess the differences between uncoated, Col-I and FN coated membranes among PDMS, 0.5% mpPDMS and 1% mpPDMS membranes. All uncoated groups are significantly different than all other groups. Other pairs of groups showing statistical significant differences are shown on the graph (*:$p<0.05$) (Days 1-7). 31

Figure 4.11 alamarBlue cell proliferation assay to assess differences between cells under static magnetic field (SMF) and controls using all experimental groups listed in Table 4.2. All membranes were coated with Col-I. All BSM groups were statistically significant different than their controls (*:$p<0.01$) (Days 1-7). 32

Figure 4.12 alamarBlue cell proliferation assay for PDMS, 0.5% mpPDMS and their BSM variants for different protein coatings (Fibronectin and Col-I). All BSM groups are statistically significant different than their controls. Except for Col-I coated PDMS and BSM PDMS ($p<0.05$), all P-values are smaller than 0.01. (Days 1-7). 34

Figure 4.13 Actin filament and nuclei of adherent cells were stained to observe effects of surface topography and protein modifications on cell behaviour and morphology. (A) Plain PDMS+FN, (B) Plain PDMS+Col-I, (C) BSM PDMS+FN, (D) BSM PDMS+Col-I, (E) BSM mpPDMS+FN, (F) BSM mpPDMS+Col-I (Day 3). 36

Figure 4.14 Actin filament and nuclei of adherent cells were stained to observe effects of surface topography and protein modifications on cell behaviour and morphology. (A) BSM PDMS+FN, (B) BSM PDMS+Col-I, (C) BSM mpPDMS+FN, (D) BSM mpPDMS+Col-I (Day 14). 37

Figure 4.15 Actin filament and nuclei of adherent cells were stained to observe effects of surface topography and protein modifications on cell behaviour and morphology. (A) Plain PDMS+FN, (B) Plain PDMS+Col-I, (C) BSM PDMS+FN, (D) BSM PDMS+Col-I, (E) BSM mpPDMS+FN, (F) BSM mpPDMS+Col-I (Day 21). 38

Figure 4.16 Actin filament and nuclei of adherent cells were stained to observe effects magnetic particle presence and protein modifications on cell behaviour and morphology. (A,B) 0.5% mpPDMS+FN, (C,D) 0.5% mpPDMS+Col-I, (E) 1% mpPDMS+FN, (F) 1% mpPDMS+Col-I (Day 7). 39

Figure 4.17 Actin filament and nuclei of adherent cells were stained to observe effects of uncoated PDMS surfaces on cell behaviour and morphology. (A) Plain PDMS, (B) 0.5% mpPDMS, (C) 1% mpPDMS (Day 3). 40

Figure A.1 Calibration curve for Bradford assay created for 0.1M Acetic acid solubility. 54

Figure A.2 Calibration curve for Bradford assay created for 0.5M Acetic acid solubility. 54

LIST OF TABLES

Table 4.1 Water Contact Angle measurements of experimental groups and controls. 24

Table 4.2 Preliminary alamarBlue assay groups. 30

LIST OF SYMBOLS

S_a	Surface roughness
S_q	Root mean square roughness

LIST OF ABBREVIATIONS

AFM	Atomic Force Microscopy
ALP	Alkaline Phosphatase
APTES	(3-aminopropyl)triethoxysilane
BMP	Bone Morphogenetic Protein
CAD	Computer Aided Design
Col-I	type I Collagen
DMEM-F12	Dulbecco's Modified Eagle Medium-F12 (1:1)
ECM	Extra Cellular Matrix
FDA	Food and Drug Administration
FN	Fibronectin
FTIR	Fourier Transform Infrared Spectroscopy
GA	Gluteraldehyde
mpPDMS	Magnetic Particle Embedded PDMS
MTT	3-(4,5-dimethylthiazol-2-yl)-2,5-diphenyltetrazolium bromide
OSC	Osteocalcin
OSX	Osterix
PBS	Phosphate Buffered Saline
PBSt	Phosphate Buffered Saline with 0.1% Tween-20
PDMS	Poly(dimethylsiloxane)
PEG	Poly(ethyleneglycol)
PGA	poly(glycolic acid)
PLA	poly(lactic acid)
PLGA	poly(lactic-co-glycolic acid)
RGD	Arginine(R)-Glycine(G)-Aspartate(D)
ROCK	Rho-associated protein kinase
Runx2	Runt-related transcription factor 2
TEM	Transmission Electron Microscopy
TGFβ	Transforming Growth Factor β

UV	Ultraviolet
VSM	Vibrating Sample Magnetometer

1. INTRODUCTION

1.1 Motivation

Bone regeneration is a physiological process of bone formation involves complex and well-organized pathways. These processes take place constantly throughout adult life and can be observed during fracture healing. In the case of more complex circumstances where greater quantities of bone regeneration is necessary for healing different strategies has to be followed to assist and further augment these healing processes via bone grafting, use of growth factors and using biocompatible scaffolds. Most commonly performed procedure to overcome severe bone related disorders is bone grafting and its gold standard is autologous bone usage. Autologous bone grafting satisfies all prerequisites such as presence of BMPs, osteoprogenitor cells to trigger osteogenesis and a scaffold to initiate osteoconduction, but it requires extra surgical operations with substantial costs and patient discomfort. An other option for bone grafting is allogeneic grafting which bypasses gathering of bone tissue from patient and enables to find an appropriate alternative from a cadaver or from another person [1]. Xenogeneic grafts, which means a tissue taken from another species, can also be used but allogeneic and xenogeneic grafts have underlying limitations such as immunogenic responses, infection, and pathogen transmission risks on transplanted patient [2]. These circumstances made researchers to lean towards to the use of biocompatible and possibly biodegradable materials, which can bypass these problems and also be designed uniquely for every patient. Healing of a damaged area can be augmented and supported externally using different types of biomaterials, designed to interact with cells in their natural environment, using biomimetic and bioinspired approaches.

Cell microenvironment is defined as biochemical and biophysical factors that have an effect on the cell behaviour. Extracellular matrix (ECM), other neighbouring cell types, bioactive agents and hormones, surface topography and mechanical forces can be collectively taken as cellular microenvironment [3]. Physical cell interaction with

this microenvironment is now known through several factors that have been detected, such as stiffness, porosity and surface roughness which directly effects focal adhesions of cells onto these surfaces [4].

Mechanotransduction can be explained as an emergent biological response from a cell, upon a physical stimilus. These mechanotransductive pathways are triggered through mechanosensitive molecules and proteins inside the cell such as integrins, ion channels and growth factor receptors. Main source of cellular mechanotransduction happens on the cell membrane where the cells are in direct contact with their ECM through focal adhesions. These focal adhesions are continuously formed by integrins and they are regimented according to the ECM protein composition, such as fibronectin, collagens and laminins [5]. Sensitivity of cells to their topographical environment affect different cell adhesion and gene expression behavior as surface properties change in a physical level [6]. Bone surface topography does not have ordered symmetries and its randomized pattern is crucial for osteoprogenitor cells to show osteospecific differentiation patterns [7]. Apart from topography biochemical composition of bone surface is also crucial for bone formation. Natural bone extra cellular matrix (ECM) consists collagen, several growth factors, hydroxyapatite (found in bone matrix) and proteoglycans. There are several methods to combine these physical and chemical properties such as modification of polymers using biochemical molecules, extracting readily formed ECM components from decellularized tissue and combining them with polymeric carriers, or static culturing on porous scaffolds to generate ECM coating [8].

Polydimethylsiloxane (PDMS) is a silicon based organic polymer. PDMS has high degrees of biocompatibility and biostability, making the polymer suitable for long term implantations [9]. This material is widely used in various fields due to its non-toxicity, optical transparency, chemical inertness [10], adjustable stiffness and its ability to be used in soft lithography [11] and its chemically modifiable surface using various methods [12]. With pattern transfer resolutions in sub-15 nm range [13], PDMS is a great candidate to be used as a bone surface topography mimicking membrane on *in vitro* cell culture studies. On the other hand, PDMS is chemically modifiable with proteins using various methods such as O_2 plasma, UV/ozone treatments and Corona

discharge [12].

Magnetic nanoparticle embedded scaffolds, along with externally applied magnetic fields, increased osteoblastic functionality. It is thought to be related to effects of static magnetic fields (SMFs) with integrins and and BMP-mediated signaling pathways [14].

PDMS is selected as a model surface and the membrane polymer because of its ability to mimic surface properties with nanometer precision via soft lithography. Moreover, it is chemically modifiable with ECM proteins such as Fibronectin and Collagen-I. Both bone surface mimicked surface topography and protein modifications were done in order to contribute to physical and chemical osteoblastic cell microenvironment. Effects of Fe_3O_4 magnetic particles embedded into PDMS membranes is also added to the study in order to investigate their effect on cellular behaviour and mechanotransduction.

1.2 Objective

Main goal of this study was to investigate the effects of bone surface topography and surface modification on osteoblastic cell behaviour, using PDMS soft lithography techniques to develop bone surface mimicked PDMS membranes. To further investigate osteoblastic behavior under weak magnetic fields, magnetic particles were embedded homogeneously inside the membranes using different concentrations. Main objectives of this study were;

- Transferring bone surface topography patterns to PDMS membranes using a soft lithography approaches.
- Synthesizing and homogeneous dispersion of Fe_3O_4 magnetic particles inside PDMS membranes.

- Modification of surfaces with bone matrix proteins, namely Fibronectin and type I Collagen.
- Investigation of change in material characteristics and osteoblast cell behaviour with different membrane surface topographies, surface protein modification and under Fe_3O_4 magnetic particle presence.

1.3 Outline

This thesis is presented as chapters in the order of; Background Information about bone structure and biology along with the information of materials used in this work, Materials and Methods presenting experimental procedures, Results and lastly Discussion where all data collected from experiments are analyzed, discussed and compared to the literature.

2. BACKGROUND

2.1 Bone structure

Bones of the skeleton support the body structure, allowing movement and motion by acting as levers for the muscles, protecting organs, helps regulation of mineral homeostasis and acid/base balance, serving as a supply of growth factors and cytokines and provide the environment for production, development and differentiation of various types of blood cells within the bone marrow [15].

From a morphological point of view bone can be defined either as trabecular or as cortical. Cortical compartment of bone structure fills up approximately 80% of the total bone mass. Vascular channels present inside this region inhabit 30% of this volume. Ratio of volume to surface is relatively higher compared to trabecular region. In the trabecular compartment 20% of the volume is composed of bone and rest of the space is filled with marrow and fat. Trabecular bone is more related with metabolic activities than cortical bone, which generally yields substantial mechanical strength [16], [17].

Trabecular bone tissue is a porous sponge-like structure, composed of soft and hard portions. They can be located at the interior parts of long bones and in the vertebrates. Hard trabecular bone mesh forms a firm structure with relatively high ductility compared to its surrounding sub-tissue, provides the framework needed for the bone marrow. In a microscopic scale, optimization of load transfer is achieved across this trabecular framework due to its properly organized structure. Mechanical properties of trabecular bone tissue is determined by its degree of mineralization, framework of trabecular struts and plates and collagen content present in this tissue [18].

As mentioned above, cortical bone constitutes approximately 80% of the total mass in the entire bone structure. Low porosity and high matrix mass per unit volume

ratio allows cortical bone to have great compressive strength, therefore; conspicuously support the mechanical role of bone. Trabecular part of the bone is enclosed by a relatively thinner cortical shell. Long bone structure constitutes from two ends of the bone (epiphysis) and cylindrical body (diaphysis). Tubular design arranges bone minerals away from the bending axes and increases bending resistance without an incidental increase in total bone mass. Rigidity provided by cortical bone allows weight load and muscular action, whereas trabecular enclosing provides porous and lightweight framework for energy efficiency during motion [19].

Periosteum is a tissue surrounding the cortical bone and consists of two distinct layers, an outer fibrous layer and an inner cambium layer with osteoblast like cells. This tissue covers majority of bones present inside the body except their joints and sesamoid bones. Formation of the bone takes place in two processes called membranous and endochronal ossification [20]. Outer layer of periosteum contains compact collagen fibers, fibroblasts and their progenitor cells whereas inner layer contains osteoblasts and osteoprogenitor cells [21]. Overall process is named skeletogenesis, and it starts with moving of mesenchymal stem cells from embryonic lineages to areas where bones would be formed. Cell densities present in those areas thought to determine the shapes and sizes of these bones. From condensed cellular clusters, mesenchymal stem cells differentiate into osteoblasts or chondrocytes to from cartilage (endochondal formation) or bone tissue (intramembranous formation), respectively [22]. Periosteum is a connective tissue located in the interfaces between bones and neighboring tissues and it is a source of progenitor cells to assist bone tissue repair and shown to accelerate healing processes of these tissues. Its inner layer is directs in contact with the bones and characterized by the shapes of osteoblasts organized in rows. Osteoblasts and preosteoblasts found inside inner periosteum secretes osteoblast-specific factor-2 as an ECM protein and thought to be a parameter of cell adhesion on these surfaces [23].

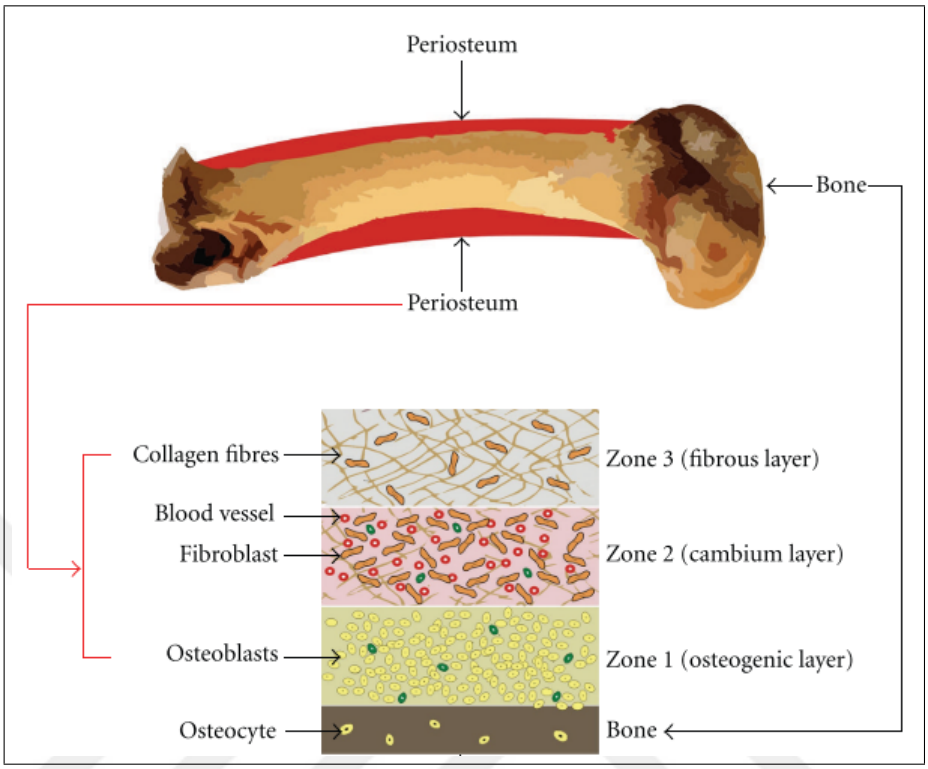

Figure 2.1 Layers of periosteum [21].

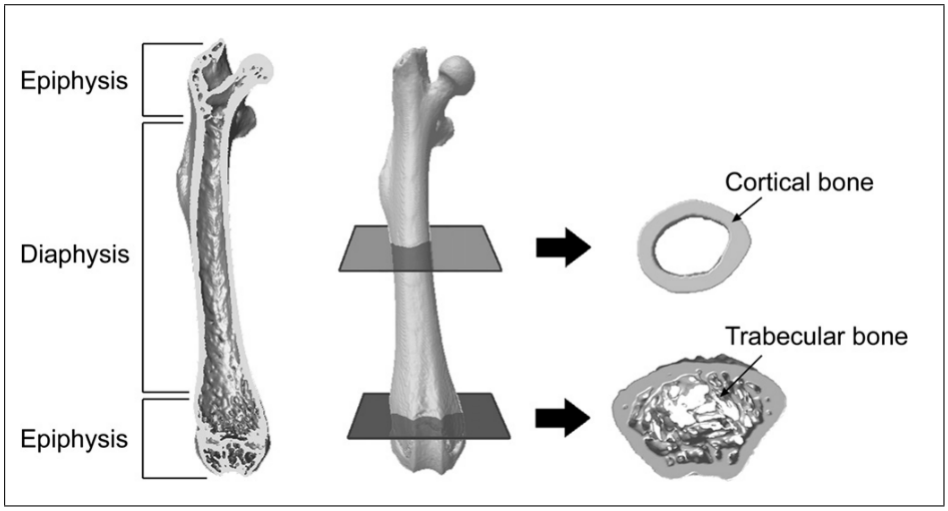

Figure 2.2 Macroscopic anatomy of bone [19].

2.2 Biology of Bone

Cellular composition of the bone includes osteoblasts, osteocytes, bone lining cells, and osteoclasts. Osteoblasts are the cells derive from mesenchymal stem cells and responsible for formation of new bone inside the body. Osteoblasts synthesize the extracellular matrix with different types of proteins with most abundant being fibrous Col-I. Bone extracellular matrix contains several growth factors such as TGFβ, BMPs, insulin like and platelet derived growth factors [24]. These cells also regulates mineralization of ECM by secretion of membrane bound vesicles that concentrate calcium and phosphate and dispatch mineralization inhibitors in the surrounding area. Osteoblasts differentiate into osteocytes with an extended canalized network linking them to the other types of cells present in the bone tissue, such as bone lining cells, osteoblasts and osteocytes, by becoming enclosed in its ECM [15]. Interestingly osteoblasts are also responsible for regulating bone resorption, even though osteoclasts are cells involved in the resorption process, due their receptors for well-known bone resorbing hormones PTH and 1,25$(OH)_2$-vitamin D3 [24].

Osteocytes are the cells differentiated from osteoblasts buried within the self created bone matrix. They are the main sensor, integrator and transducer of the skeleton. Along with the other cell types present inside the bone, osteoblasts, osteoclasts and bone lining cells, they are also responsible for the growth, maintenance and healing of the bone. Osteocytes contact other osteoblasts, bone marrow, and other osteocytes through tubular canaliculi via their dendrites and they constitute the living network within the mineralized matrix. To increase adaptation to the environment these cells across the bone are organized in a three dimensional way and form the bone membrane and cell matrix interface [25]. They reside inside the lacunae under the mineralized bone matrix. Network formed by these cells is called lacunocanacular network and it is the main path to provide nutrients and oxygen to maintain viability [26].

Osteocytes are distributed inside the bone membrane ideally to sense mechanical loads applied onto the bone [18]. Their mechanosensitive function is established due to their location inside the matrix. Shape and spatial composition of these cells express

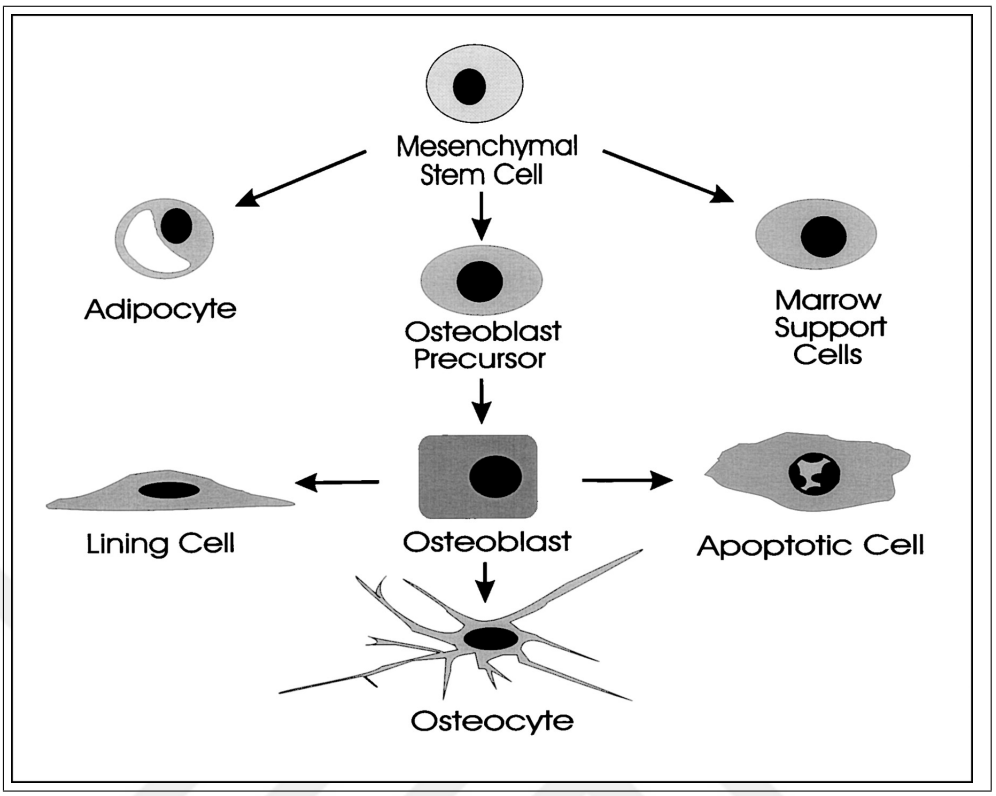

Figure 2.3 Osteogenic pathways of mesenchymal stem cell differentiation [27].

biochemical signals upon mechanical stimulus. There are two proposed explanations of this mechanotransductive pathway. One of them is expression of proteins upon stimulus said to be important to maintain mechanotransductive signalling and bone formation, PolyCystins 1 and 2. The other proposed pathways is producing secondary messengers after stimulation such as ATP, Nitric Oxide (NO), Ca^{2+} and prostaglandins. Regardless of the pathway, mechanotransductive functionality is possibly made possible by the canalicular network [28].

2.3 Cellular Microenvironment

Cell microenvironment can be defined as the biochemical, biophysical and biomechanical factors that affect cell behavior. These effects include ECM, other neighboring cells, hormones, cytokines and similar chemical factors, surface topography and mechanical forces acting upon cells [3]. This microenvironment plays crucial roles migra-

tion, proliferation, differentiation and apoptosis [29]. Cell microenvironment changes depending on the cell function and location. For example, cellular microenvironment for stem cells might dictate whether if the cell differentiates, proliferates or dies according to the soluble factors effecting intracellular pathways [30].

However, recreating this microenvironment proves to be challenging due to the numerous factors in play such as mechanical stimuli that are generated on the cell from atmospheric pressure, 3D nature of natural cell microenvironments present compared to usual 2D environment of *in vitro* studies. Especially for bone microenvironment mimicking, mechanical factors such as stiffness and porosity is hard to replicate [31]. It should be also remembered that the natural microenvironment constantly changes and an exact replication remains challenging.

2.4 Biomaterials used in Bone Regeneration Applications

Biomaterials being used in bone regenerative medicine can be classified under three main types, natural polymers, synthetic polymers and inorganic materials. Each subtype of these materials (Metals, bioceramics, natural and synthetic polymers etc.) have their advantages and disadvantages [32]. Metallic biomaterials are commonly used in bone healing treatments and research are Titanium (Ti) and Tantalum (Ta) and their alloys due to their great mechanical properties and porous structure allowing cell growth [33]. Ceramics are used as a biomaterial to develop 3D scaffolds from various materials such as hydroxyapatite and tricalcium phosphate. They are inorganic components of the bone tissue and also release calcium ions while degrading. These materials are biocompatible and also osteoinductive; therefore, they are used in various bone tissue engineering studies as well [34]. Some polymers are widely used as membranes in bone tissue related research due to their wide range of properties and biocompatibility. Naturally available polymers such as starch and alginate or proteins such as collagen and silk are degradable and biocompatible [35]. Synthetic polymers such as poly(lactic acid) (PLA), poly(glycolic acid) (PGA) and their combination poly(lactic-co-glycolic acid) (PLGA) are also being used as membranes in bone regeneration research. They

are FDA approved, have controllable degradation rates are easily produced [36].

All these materials have their disadvantages as well such as metals are not biodegradable and may corrode to present toxicity. Ceramics have a better range of mechanical properties but they are brittle and they may fracture. Polymers have their controllable degradation properties but they usually lack necessary mechanical strength to be used in applications for bone tissue [37]. Therefore, there is no perfect biomaterial in every aspect and one should pick the most suitable material and modify its properties for the field of study.

2.5 Properties of Polydimethylsiloxane (PDMS)

Polydimethylsiloxane (PDMS) is a relatively inexpensive material with adjustable mechanical properties, gas permeability, little auto fluorescence, ability to be used in soft lithography applications and nano-scale pattern mimicking precision [38]. It is a strong, flexible and elastically deformable ductile material with a wide range of use in fields like making valves and pumps, microfluidics and in biological studies [39]. Any desired design of a micro-structure can be transferred onto the PDMS structures using CAD softwares by printed that desired design transparencies. These transparencies are then used as photomasks and transferred onto silicon wafers using UV-photolithography, creating a silicon wafer master mold. These molds can be used afterwards to transfer the patterns onto PDMS structures using soft lithography [40].

Furthermore, PDMS is transparent and bio-compatible. Along with its gas permeability, and adjustable stiffness, PDMS membranes are widely used on cell biology studies [41]. One major downside of PDMS is its hydrophobic nature (Water contact angle $>100°$) [39]. To overcome this effect methods such as oxygen plasma treatment to create hydroxyl groups on the polymer surface [42], UV/ozone treatment to break methyl groups on backbone structure of PDMS and replace them with silanol groups [43], and using corona discharges to creation of hydroxyl groups [44]. Even though these methods decrease surface water contact angle, they are not permanent and structure

retains its hydrophobicity due to hydrophobic recovery [45]. Several methods of post treatments after surface activation have been reported to preserve hydrophilicity of the PDMS structure, such as PEG and HEMA grafting of PDMS surfaces aiming to lower zeta potentials of structure and retaining surface hydrophilicity [46]. Another study have shown that PDMS surface grafting using various materials such as acrylic acid, acrylamide, dimethylacrylamide, 2-hydroxylethyl acrylate, and poly(ethylene glycol)-monomethoxyl acrylate have been successfully grafted onto PDMS surface after UV exposure and decreased surface hydrophobicity [47], allowing its use in different areas such as in microfluidic devices and cell culturing experiments. Other methods to modify PDMS surfaces after surface activation include chemical vapor deposition, silanization, grafting-to and -from methods to attach functionalized polymer chains onto reactive sites and initiating polymerization on the surface, respectively [12].

2.6 Effects of magnetism on cell metabolism

Natural geomagnetic field is between 20-70 μT over the Earth surface and living organisms are constantly being affected from this magnetic field. It is implicated that some animal species even migrate according to fluctuation of this magnetic fields [48]. Static Magnetic Fields (SMF) are a type of magnetic field usually generated from metals with magnetic properties. They are non-invasive, not being generated from a device powered with electricity. They also do not cause any change in temperature or any electrical hazard on the target tissue [49]. Application of magnetic fields are readily being used in various bone related diseases or dysfunctionalities such as fracture healing, spinal fusion, osteoarthritis and wound healing.

Generally, effects of these magnetic fields are closely related to the type of cell line. It was reported that cell proliferation stood unaffected for 21 days up under magnetic fields up to 1.5T for the human fetal lung fibroblasts [50]. Another study suggests that human skin fibroblasts change their morphology under 0.2 T magnetic fields, thought to be related to charged sugar residues modify on cytoskeleton arrangement under 0.2 T magnetic field, but their proliferation potential didn't change [51].

Effects of magnetic fields on osteoblastic cell behaviour had been studied and observed over past decade. These effects include, an increased rate of osteoblast proliferation using pulsed electromagnetic fields (PEMF) [52], promotion of osteoblast differentiation using electrostatic field induction devices (EFID) [53], increase in alkaline phosphatase secretion and a change in Col-I and FN expressions under large-gradient high magnetic fields [54]. Also an increase in osteocalcin up until day 3 was reported under static magnetic field exposure for an hour each day but this effect was reversed after day 7. In addition to this, continuous exposure resulted in a decrease in osteocalcin secretion. Quantitative PCR results have also shown that osteoblastic markers were unaffected from applied magnetic fields and cell morphologies haven't been effected [55]. It can be concluded that there are alterations in cell biology under applied magnetic fields but there isn't a definitive conclusion and more studies should be made for better understanding of these possible effects.

3. MATERIALS AND METHODS

3.1 Bone Xenograft Cleaning

Bone pattern used in this study was obtained from bovine femur. Bovine femur bone was purchased from a local butcher and chemically cleaned using xenograft cleaning process [56]. Bone chips were obtained by cutting bovine femur using a bone saw and placed inside absolute ethanol for 30 minutes and transferred into a 10% NaCl solution for 24h with first and last 20 minutes inside an ultrasonic bath to remove cells and tissue remaining on the bone surface. Bone chips were then placed inside acetone for 20 minutes to remove lipids and possible residues from surface. To remove immunologic structures and inactivate prions, bone chips were immersed into 3% H_2O_2, 2 M NaOH and acetone for 72 h, 2 h, and 144 h respectively. Chemically cleaned bone chips were left to dry overnight and used in soft lithography. Schematic showing the cleaning process with details are given in Figure 3.1.

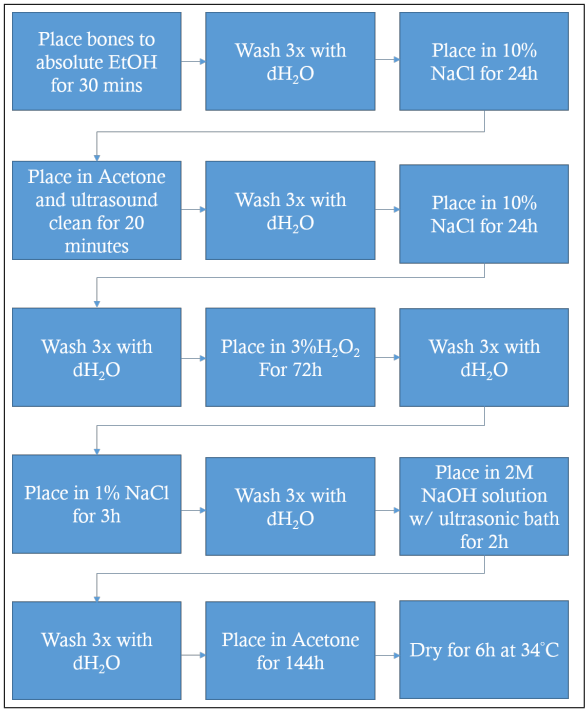

Figure 3.1 Schematic of xenograft bone cleaning process.

3.2 Magnetic particle synthesis

Magnetic particles used in this study were synthesized using co-precipitation method (Figure 3.2). 125 mL of 1.5 M NaOH solution was prepared and placed inside a container. Reactive solution was prepared by combining iron (Fe) salts by adding 0.6627 g $FeCl_24H_2O$, 1.083 g $FeCl_36H_2O$, 3.4 mL 12.1 M HCl and 80 mL dH_2O together and stirring until salts were dissolved solution color turned to yellow. Under constant N_2 atmosphere and mixing at 1200rpm, salt solution was added to reaction chamber drop-wise at 80 °C. After entire acidic salt solution was added, mixture was left to stir for 20 minutes. Synthesized magnetites (Fe_3O_4) were precipitated using a neodymium magnet and supernatant was removed. Magnetites were suspensed with 0.01M HCl inside microcentrifuge tubes and centrifuged at 14000 rpm for 15 minutes twice. Magnetites were then resuspended with dH_2O. Suspensions were dried at 50 °C overnight on a glass petri dish and scraped after drying.

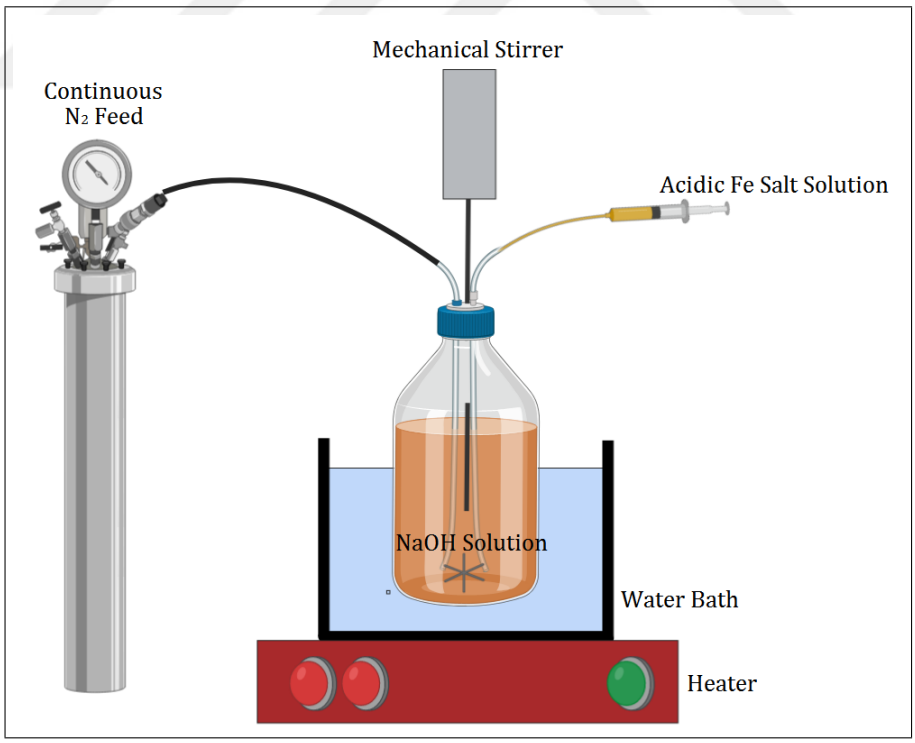

Figure 3.2 Schematic of magnetic particle synthesis.

3.3 Production of PDMS Membranes

3.3.1 Preperation of plain PDMS membranes

PDMS membranes were prepared by mixing silicon elastomer and curing agent with a 10:1 ratio (w/w) (Sylgard 184, Dow Corning, US). This mixture was degassed inside a vacuum chamber until air bubbles were completely removed and poured onto a glass surface and heat cured at 70 °C for 4 hours. Cured PDMS was peeled off and cut according to desired size and shapes. Preparation of magnetic particle embedded PDMS membranes (mp-PDMS): Magnetic particles (Fe_3O_4) were added into curing agent and homogenized using a digital homogenizer (Omni Ruptor 4000, Omni International, US) for 20 minutes inside an ice bath to avoid heating of curing agent. This mixture was mixed with silicon elastomer 10 times the weight of curing agent used in magnetic particle dispersion to obtain 10:1 ratio (w/w) and stirred vigorously for 5 minutes. PDMS prepolymer containing magnetic particles was degassed inside a vacuum chamber until air bubbles were removed completely and poured onto a glass surface and heat cured at 70 °C for 4 hours. Prepared magnetic particle (Fe_3O_4) embedded PDMS membranes is given in Figure 3.4.

3.3.2 Preperation of Bone surface mimicked PDMS membranes (BSM PDMS)

Negative bone surface mimicked PDMS membranes were obtained by transferring bone surface patterns onto PDMS membranes using soft lithography. These negative molds were coated with a thickness of 40 nm with gold (Au) using a sputter coater (Polaron SC 7640 Sputter Coater, Quorum Technologies, UK). Gold coated negative PDMS membranes were immersed into PDMS prepolymer and degassed by displacing membranes inside prepolymer and degassing repeatedly until all air bubbles under negative molds were removed. PDMS was cured at 70 °C for 4 hours. After curing process positive patterned PDMS membranes were collected from gold coated molds by peeling gently. Entire process is visualized in Figure 3.3, and obtained BSM

PDMS membranes can be seen in Figure 3.5.

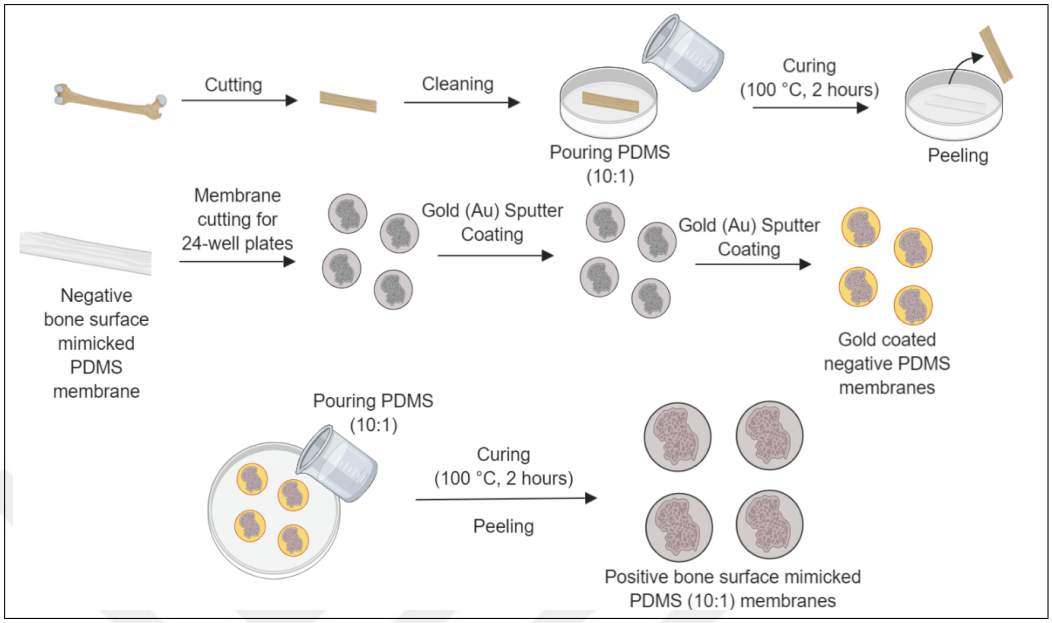

Figure 3.3 Preperation of BSM PDMS membranes.

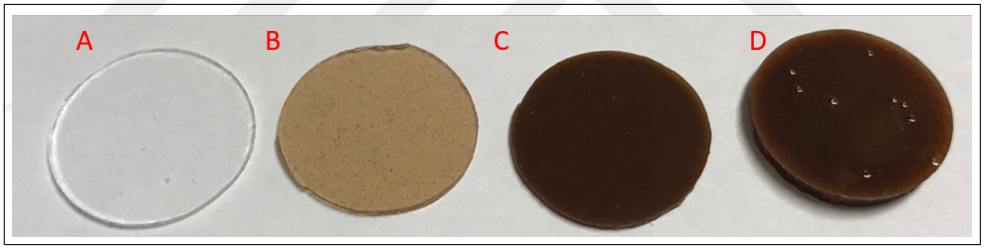

Figure 3.4 PDMS membranes with different concentrations of magnetic particles embedded. (A) Plain PDMS, (B) 0.5% mpPDMS, (C) 1% mpPDMS, (D) 2% mpPDMS.

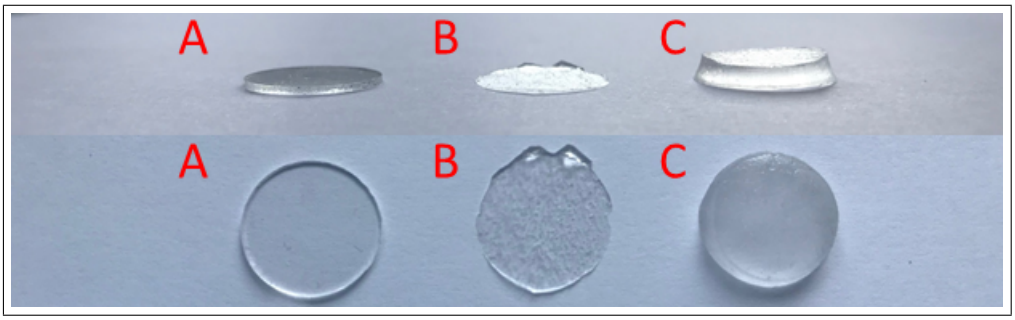

Figure 3.5 PDMS membranes with different approaches of bone surface mimicry. (A) Plain PDMS, (B)BSM PDMS,(C)BSM PDMS (before optimization).

3.4 Protein Modification

Both Collagen-I and Fibronectin modifications were done as reported previously [57]. PDMS surfaces were treated with O_2 plasma and silanized in 10% (3-aminopropyl)triethoxysilane (APTES) at 50 °C for 2 hours. APTES solution was removed and membranes were washed twice with dH_2O. Membranes were further crosslinked with 2.5% Gluteraldehyde (GA) solution for an hour. Membranes were washed twice with dH_2O and modified with either 0.5 mg/mL Fibronectin or Collagen-I overnight at 4 °C.

3.5 Material Characterization

3.5.1 Water Contact Angle Measurements (WCA)

Water contact angles of PDMS membranes were measured using was Contact Angle Measurement Instrument (CAM 100, KSV). Deionized water droplets (10 μL) were dropped onto different experimental groups and water contact angles were measured by circle fitting. Water contact angles for PDMS, BSM PDMS, Negative BSM PDMS, 0.5% mpPDMS, 1% mpPDMS, PDMS+Col-I, PDMS+FN, BSM PDMS+Col-I, BSM PDMS+FN, 0.5% BSM mpPDMS and 1% BSM mpPDMS were measured. Protein coated membranes were modified with their respective protein, 24 hours before measurements.

3.5.2 Transmission Electron Microscopy (TEM)

Images of synthesized magnetic particles were gathered using TEM (Tecnai G2 20 TWIN, FEI Company, US). LaB_6 electron emitter was used and images were taken at a emission voltage of 200 kV.

3.5.3 Vibrating Sample Magnetometer (VSM)

Magnetic properties of PDMS, 0.5% mpPDMS and 1% mpPDMS membranes were characterized using vibrating sample magnetometer (S700X SQUID Magnetometer, Cryogenic Limited, UK). Before the measurements, all membranes were magnetized at room temperature until they became magnetically saturated and their magnetic curves were obtained.

3.5.4 Investigation of Membrane Topographies

Surface topographies of plain and BSM PDMS membranes were investigated with SEM imaging (Philips XL30 ESEM-FEG/EDAX). Membranes were sputter coated with gold (Au) (Polaron SC 7640 Sputter Coater, Quorum Technologies, UK) and imaged at 5 kV with 100x and 2500x magnifications.

3.5.5 Atomic Force Microscopy (AFM)

Surface topography profiles along with the values for surface roughness and root mean roughness of plain PDMS and BSM PDMS were obtained from contact force modulation mode AFM imaging (AFM-Nanosurf Flex-5) using LFMR and Contscr probes, respectively.

3.5.6 Fourier Transform Infrared Spectroscopy (FTIR)

Fourier Transform Infrared Spectroscopy (FTIR) spectra was obtained to document chemical composition of PDMS membranes (Alpha FTIR, Bruker, MA, US). FTIR absorption spectra for different concentration of magnetic particle embedded PDMS membranes were presented as Transmittance vs. Wavenumbers. Measurements were taken between 600 cm^{-1} and 4000 cm^{-1} for protein characterizations for PDMS, PDMS+Col-I and PDMS+FN. For material characterizations, measurements were taken between 500 cm^{-1} and 4000 cm^{-1} for PDMS, 0.5% mpPDMS and 1% mpPDMS.

3.6 Cell culture studies

Human fetal osteoblast was obtained from ATCC (hFOB 1.19 ATCC CRL-11372 Homo sapiens bone) and used between passage numbers 6 and 9. Samples were cultured with complete DMEM-F12 medium containing 10% FBS 1% antibacterial/antimycotic solution and 1% L-Glutamine.

3.6.1 Indirect MTT Cytotoxicity assay

To assess possible cytotoxic effects of magnetic particle embedded PDMS membranes, an indirect MTT assay was performed. Magnetic particle embedded PDMS membranes with different magnetic particle concentrations (0.5% w/w, 1% w/w and 2% w/w) were sterilized with 70% ethanol and UV treated for 30 minutes. Membranes were washed twice with 1x PBS and placed inside serum free DMEM-F12 (89% v/v) supplemented with FBS (10% v/v) and antibacterial/antimycotic solution (1% v/v) for 24 hours inside an incubator. Human fetal osteoblast (hFOB 1.19 ATCC CRL-11372 Homo sapiens bone) cell line was cultivated using respective culturing medium with magnetic particle embedded PDMS membranes prepared. MTT assay was performed on 48th and 72nd hours by adding 50 μL of 5 mg/mL MTT solution in PBS into each

well. After 3 hours of incubation, MTT solution was aspirated and 400 μL DMSO was added to each well and shaked gently to dissolve formazan crystals. Absorbances were measured with a microplate reader (iMark Microplate Absorbance Reader, BioRAD Laboratories, CA, US) at 570nm wavelength, with a reference wavelength of 750nm.

3.6.2 alamarBlue cell proliferation assay

2.5 x 10^4 hFOB human osteoblast cells were seeded on PDMS, mpPDMS, BSM PDMS and mpPDMS membranes inside a 24-well plate. For the elimination study, amounts of cells seeded per well was 1.8 x 10^4 At the days 1, 3 and 7, culturing medium was aspirated and alamarBlue solution (BioRAD Laboratories, CA, US) was diluted to 1:10 with DMEM-F12 and added onto samples. After 3 hours of incubation, reduced alamarBlue solutions were transferred into a 96-well plate aseptically and samples were resuspended with fresh medium. Measurements were taken at 570nm excitation filter and 600nm emission filter using a microplate reader (iMark Microplate Absorbance Reader, BioRAD Laboratories, CA, US) and obtained absorption data was analyzed using manifacturers guidelines.

3.6.3 Flourescent Imaging

Samples were fixed on days 3, 14, and 21 in 4% formaldehyde solution for 15 minutes. Adherent cells on PDMS membranes were permeabilized in 0.1% Triton-X for 10 minutes and blocked with 1% BSA in PBSt for 20 minutes. Actin filaments were stained with phalloidin (Alexa Fluor 488 Phalloidin, ThermoFisher Scientific, MA, US), prepared by diluting 15 μL of methanolic stock solution in per mL of 1% BSA solution. For nuclear localization, cells were counter stained with DAPI. Images were taken in blue excitation filter for F-actin and violet excitation filter for nuclei stainings. Magnetic particle embedded flat membranes were turned upside down in order to avoid absorbance of excitation light by magnetic particles. Obtained images were merged using ImageJ software.

4. RESULTS

4.1 Material Characterization

4.1.1 Magnetization Measurements

Measurements for magnetization curves for plain PDMS, 0.5% mpPDMS, 1% mpPDMS membranes are given in Figure 4.1. Measurements resulted in saturation magnetizations of 0.15 emu/g and 0.30 emu/g for 0.5% mpPDMS and 1% mpPDMS, respectively. Both magnetic particle embedded membranes have shown to be super-paramagnetic.

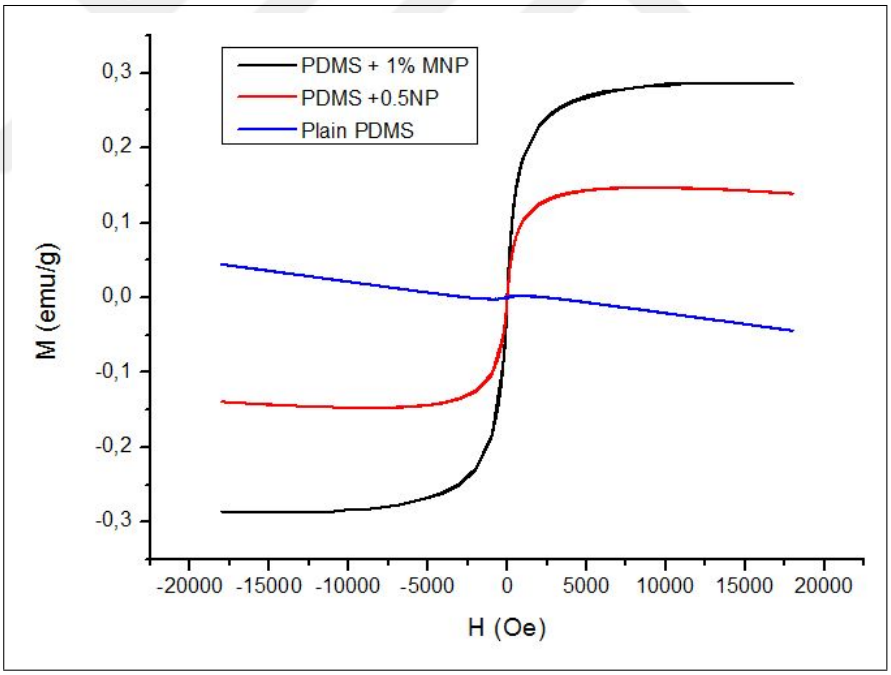

Figure 4.1 Magnetization measurements of PDMS membranes with different magnetic particle concentrations.

4.1.2 Water Contact Angle Measurements

Water contact angles of PDMS membranes were measured using Contact Angle Measurement instrument (CAM 100, KSV). Water contact angles for PDMS, BSM PDMS, Negative BSM PDMS, 0.5% mpPDMS, 1% mpPDMS, PDMS+Col-I, PDMS+FN, BSM PDMS+Col-I, BSM PDMS+FN, 0.5% BSM mpPDMS and 1% BSM mpPDMS were measured. Results were presented in Table 4.1 an images for water contact angles for different PDMS membranes were given in Figure 4.2.

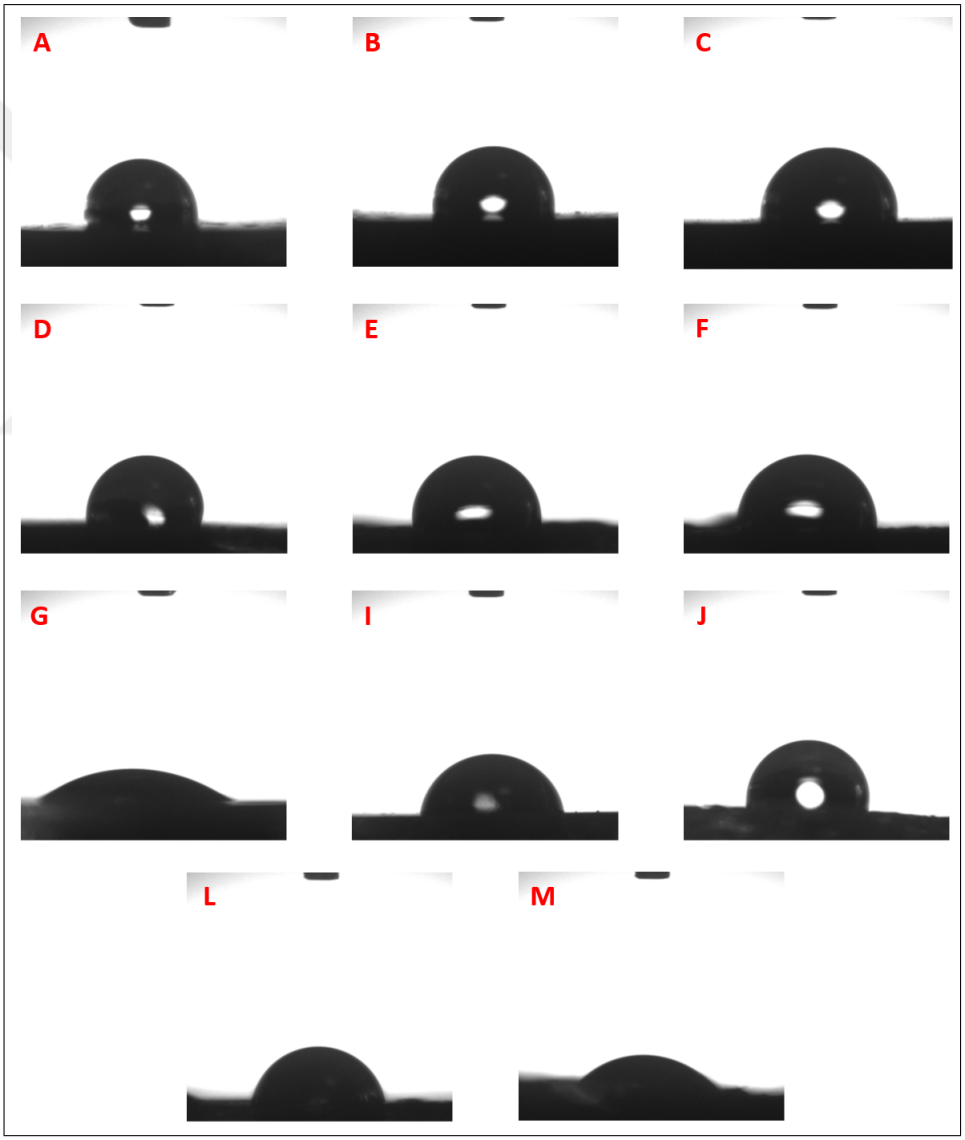

Figure 4.2 Water contact angle images of PDMS membranes with different topography and protein modifications (A) Plain PDMS, (B) 0.5% mpPDMS, (C) 1% mpPDMS, (D) BSM PDMS, (E) 0.5% BSM mpPDMS, (F) 1% BSM mpPDMS, (G) Plain PDMS+Col-I, (I) Plain PDMS+FN, (J) Negative BSM PDMS, (L) BSM PDMS+Col-I, (M) BSM PDMS+FN.

Table 4.1
Water Contact Angle measurements of experimental groups and controls.

Experimental Groups	Average [°]	St.Dev
PDMS	104.98	4.83
BSM PDMS	104.22	3.87
Negative BSM PDMS	108.00	3.99
0.5% mpPDMS	107.04	8.25
1% mpPDMS	102.14	2.10
PDMS+Col-I	32.98	8.23
PDMS+FN	66.29	3.06
BSM PDMS+Col-I	47.60	24.82
BSM PDMS+FN	53.70	6.03
0.5% BSM mpPDMS	103.70	9.49
1% BSM mpPDMS	103.91	9.49

4.1.3 Atomic Force Microscopy (AFM)

Surface profiles of plain PDMS and BSM PDMS are obtained from AFM and presented in Figure 4.3. Surface roughness (S_a) for plain PDMS and BSM PDMS membranes are 3.01 nm and 223.04 nm, respectively. Root mean square roughness (S_q) for plain PDMS and BSM PDMS membranes are 6.22 nm and 292.05 nm, respectively.

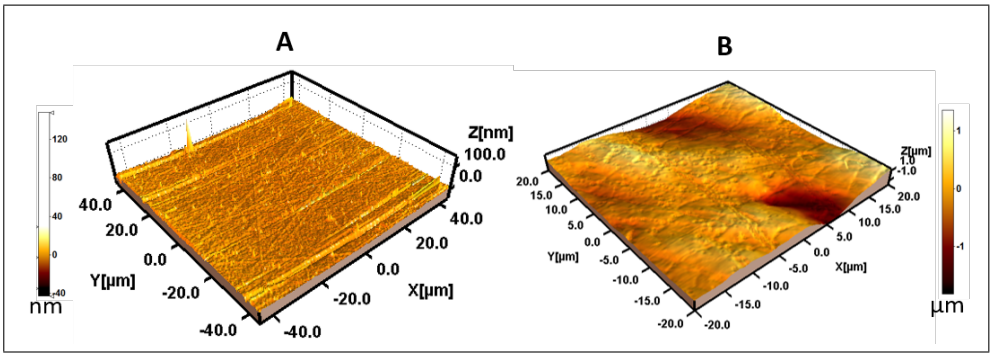

Figure 4.3 AFM surface profile for different PDMS membranes. (A) Surface profile for Plain PDMS membrane, (B) Surface profile for BSM PDMS membrane.

4.1.4 Transmission Electron Microscopy (TEM)

Magnetic particles (Fe_3O_4) synthesized using the schematic given in Figure 3.2 were investigated using TEM. Image for synthesized magnetic particles is given in Figure 4.4. Average particle size and size distribution of magnetic particles is presented in Figure 4.5.

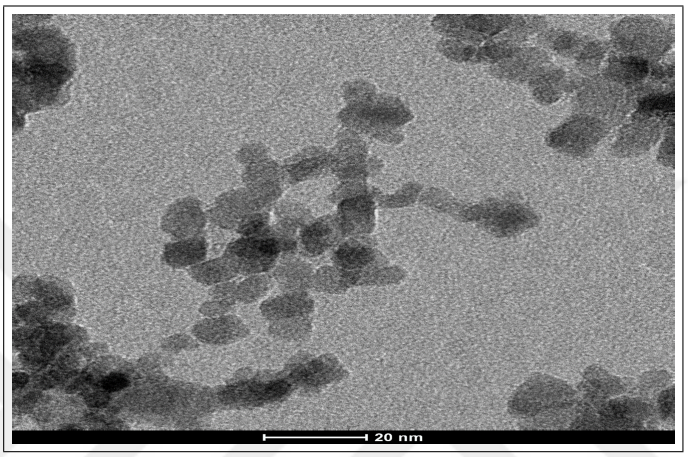

Figure 4.4 TEM image of synthesized magnetic particles (Scale bar: 20nm).

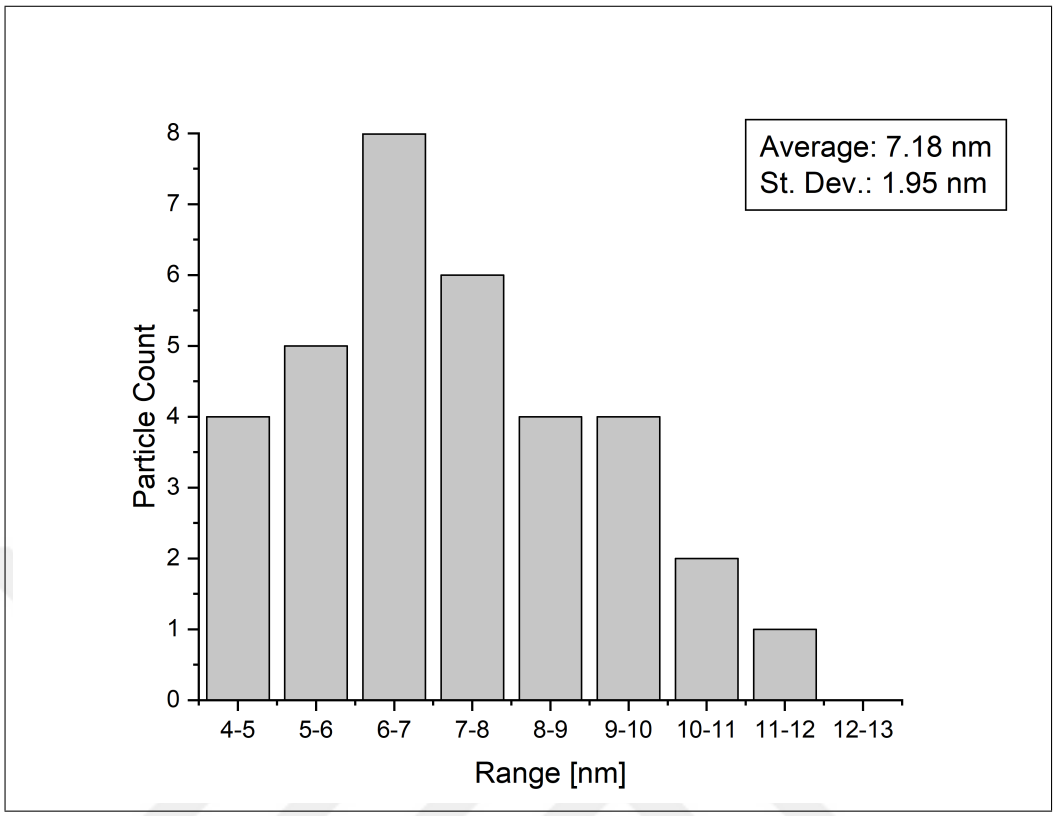

Figure 4.5 Histogram of the TEM image of magnetic nanoparticles, showing the number of particles counted in different size ranges. Average particle size and standard deviation is given on the graph.

4.1.5 Investigation of Membrane Topograpies

PDMS membrane surfaces were imaged using SEM with various magnifications to investigate surface topographies and also to verify pattern transfer quality of PDMS membranes.

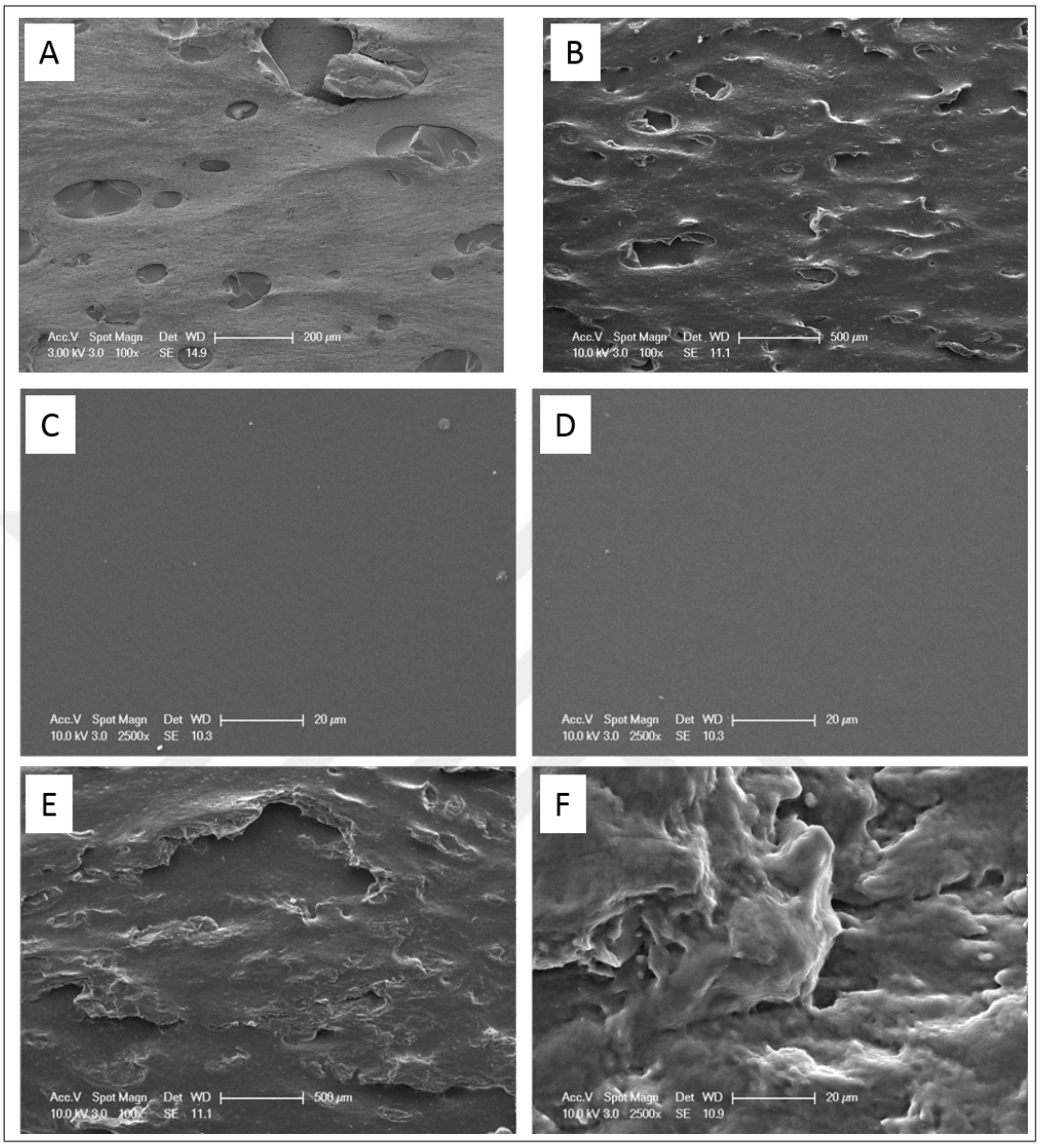

Figure 4.6 Comparison of surface topographies of bovine femur bone, BSM PDMS membranes and plain PDMS membranes. (A) Bovine Femur Bone, (B) BSM PDMS membrane. (C),(D) Plain PDMS membranes (2500x), (E) BSM PDMS membrane (100x), (F) BSM PDMS membrane (2500x).

4.1.6 Fourier Transform Infrared Spectroscopy (FTIR)

FTIR spectra of plain PDMS, 0.5% mpPDMS and 1% mpPDMS were presented in the Figure 4.7. FTIR spectra of Col-I and FN modified membranes are presented in Figure 4.8. To better view the characteristic bands, magnified versions are also presented inside the spectra.

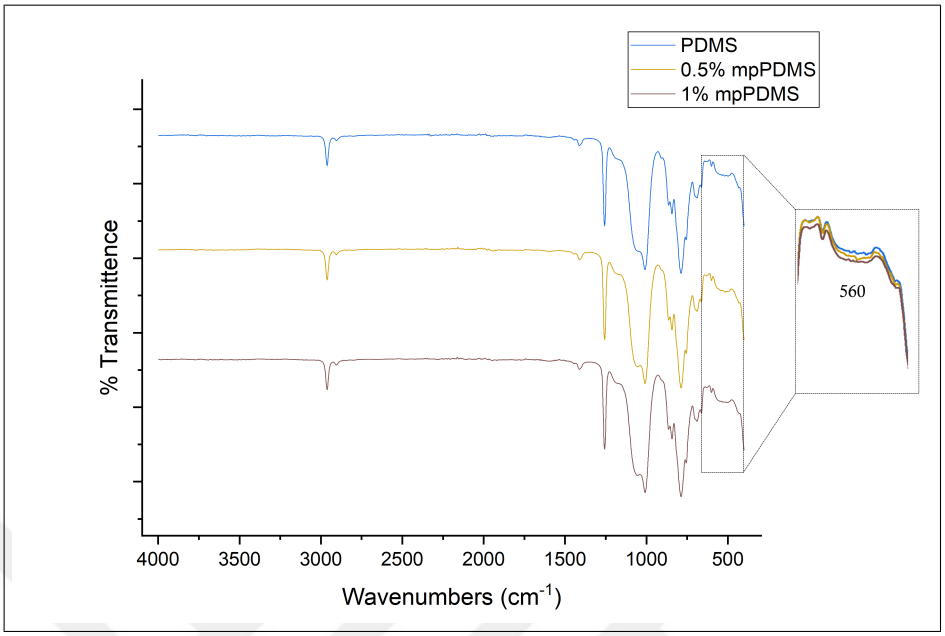

Figure 4.7 FTIR Spectra of plain PDMS, 0.5% mpPDMS and 1% mpPDMS membranes. Characteristic Fe-O bands were enlarged for visibility.

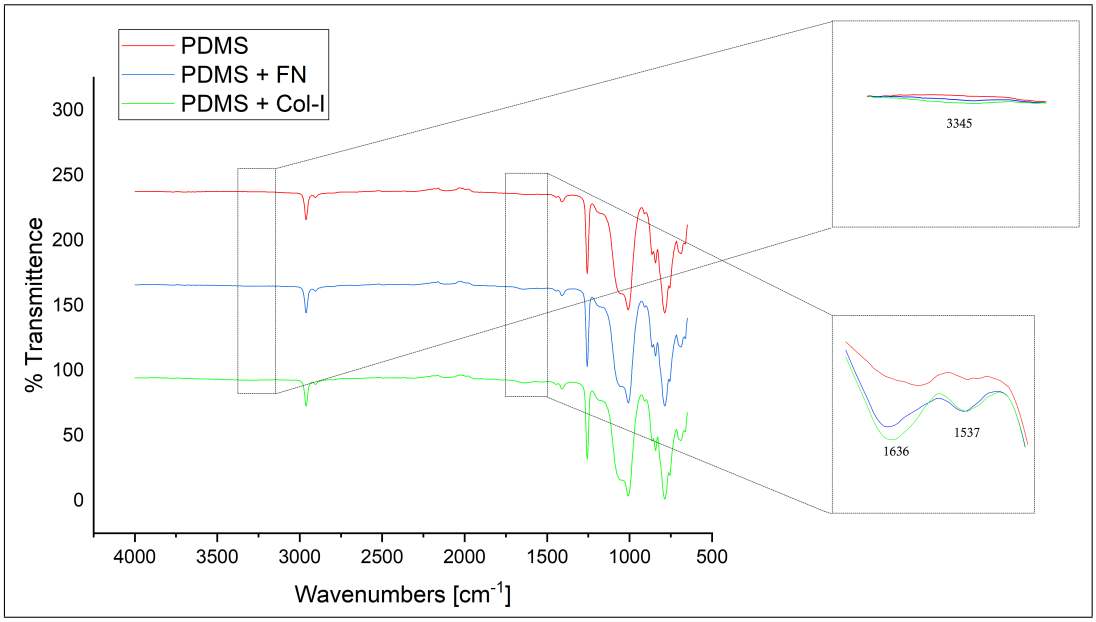

Figure 4.8 FTIR Spectra of PDMS, PDMS+FN and PDMS+Col-I membranes. Secondary amine band around 3345 cm^{-1}. Protein specific bands were enlarged for visibility.

4.2 Cell Culture Studies

4.2.1 Indirect MTT cytotoxicity assay

Cytotoxic effects of PDMS, 0.5% mpPDMS, 1% mpPDMS and 2% mpPDMS were investigated with an indirect MTT assay. Cells were seeded on 24-well plates using different DMEM-F12 cell culturing media which had been incubated with different concentration of mpPDMS for 24 hours. Results are presented in Figure 4.9. There were no statistically significant differences between cell viabilities on both day 2 and day 3.

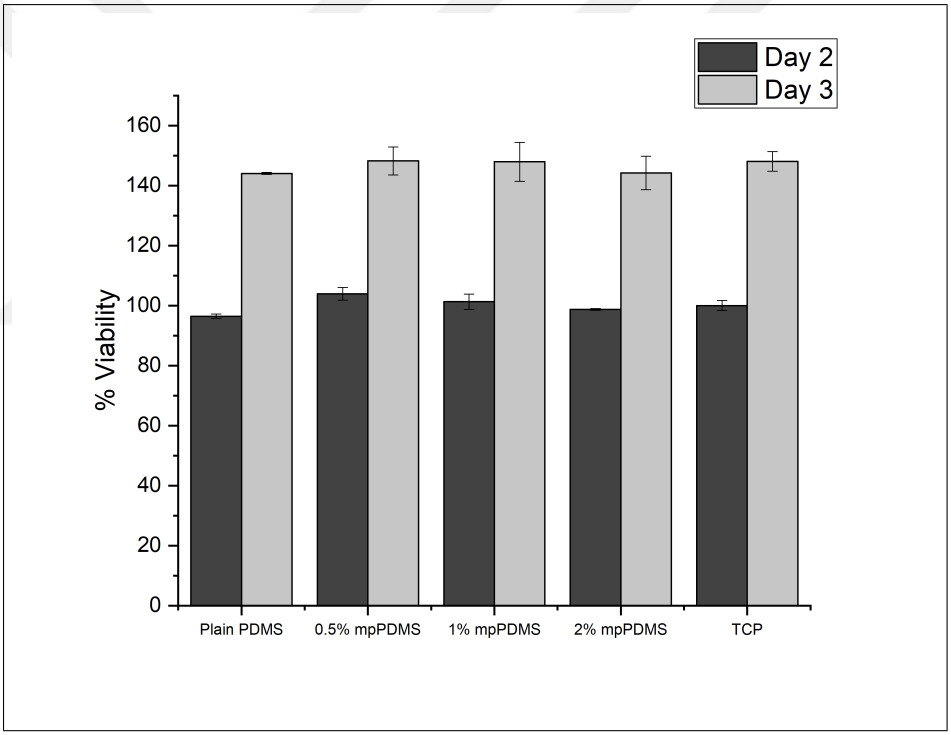

Figure 4.9 Indirect MTT cytotoxicity assay.

4.2.2 Elimination studies

To eliminate groups that will either decrease proliferation or replicate certain trends compared to groups that would yield more meaningful results, two different alamarBlue assays were conducted among the groups listed in Table 4.2 and shown on

Figure 4.10 and Figure 4.11. All adherent cells on coated membranes had significantly proliferation rates compared to cells on uncoated membranes (Figure 4.10). All BSM groups were significantly different than their controls ($p<0.01$). Cell proliferation on 1%mpPDMS membranes follows a declining trend. Plain PDMS groups maintained their proliferation levels. There were no statistical significant difference between the magnetic and non-magnetic field groups (Figure 4.11). On spite of these results, magnetic field and 1% mpPDMS groups were eliminated and 0.5% mpPDMS is selected as the sole magnetic particle embedded group for rest of the study.

Table 4.2
Preliminary alamarBlue assay groups.

	Static Magnetic Field	Control
Group 1	PDMS	PDMS
Group 2	PDMS BSM	PDMS BSM
Group 3	0.5% mpPDMS	0.5% mpPDMS
Group 4	0.5% BSM mpPDMS	0.5% BSM mpPDMS
Group 5	1% mpPDMS	1% mpPDMS
Group 6	1% BSM mpPDMS	1% BSM mpPDMS
Group 7	TCP	TCP

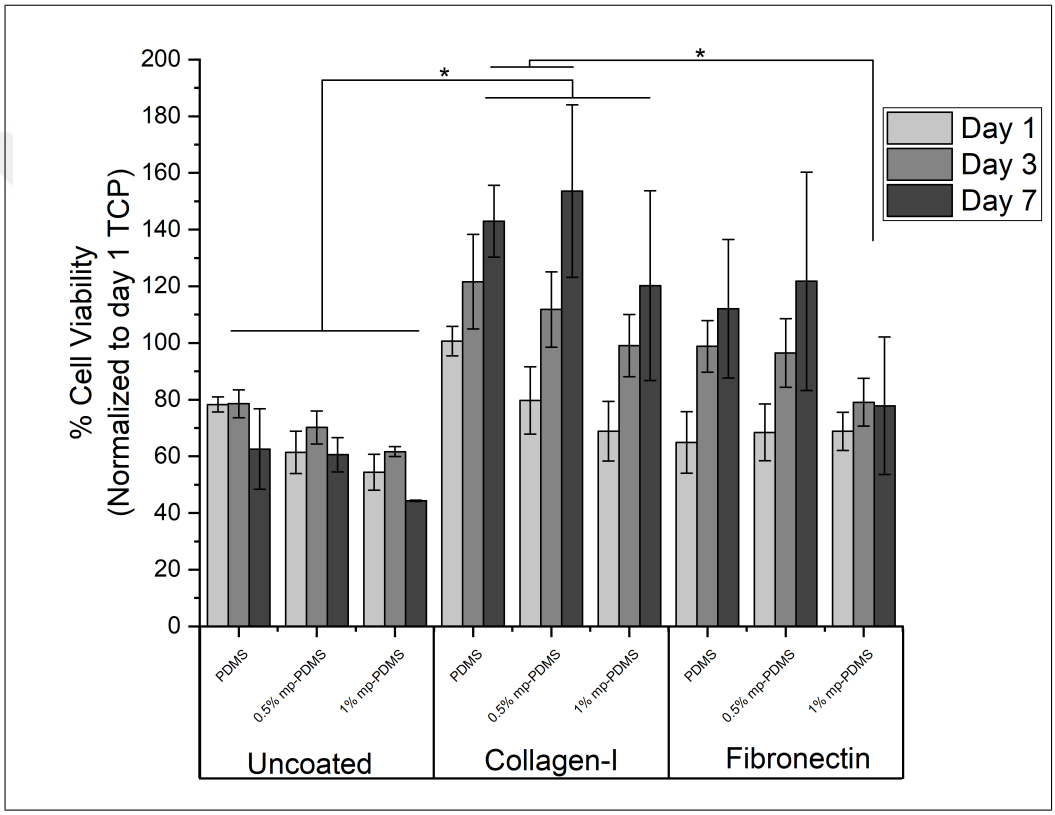

Figure 4.10 alamarBlue cell proliferation assay to assess the differences between uncoated, Col-I and FN coated membranes among PDMS, 0.5% mpPDMS and 1% mpPDMS membranes. All uncoated groups are significantly different than all other groups. Other pairs of groups showing statistical significant differences are shown on the graph (*:$p<0.05$) (Days 1-7).

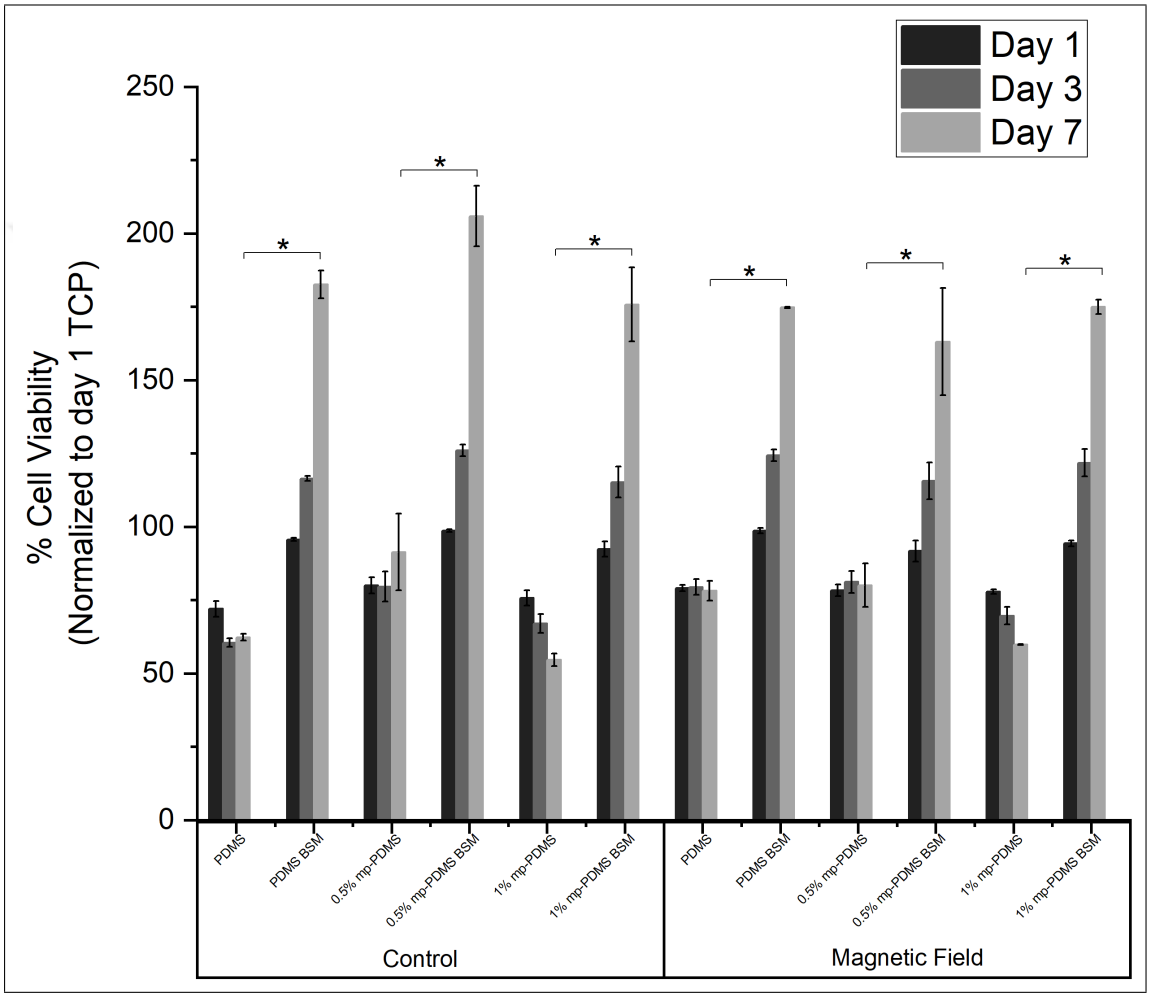

Figure 4.11 alamarBlue cell proliferation assay to assess differences between cells under static magnetic field (SMF) and controls using all experimental groups listed in Table 4.2. All membranes were coated with Col-I. All BSM groups were statistically significant different than their controls (*:$p<0.01$) (Days 1-7).

4.2.3 alamarBlue Cell proliferation assay

Cell proliferation rates of osteoblast cells were measured using alamarBlue cell proliferation assay. Resazurin, a weak fluorescent dye, present inside alamarBlue solution take electrons from electron transport chain enzymes such as nicotinamide adenine dinucleotide and reduces into resofurin, a pink highly fluorescent molecule. Increased metabolic activity yields more reduction, therefore increased fluorescence represents higher levels of viability [58]. Cell proliferation on different biochemically modified membranes were observed over 7 days with alamarBlue cell proliferation assay. On the surfaces with bone surface topography, osteoblast cells have shown higher proliferation rates compared to their plain counterparts. Differences of Fibronectin and Collagen-I was also observed. Plain PDMS membranes modified with Fibronectin are significantly different ($p<0.05$) than those modified with Collagen-I. Plain PDMS membranes with embedded magnetic particles have effected cell metabolism whereas BSM PDMS membranes with embedded magnetic particles didn't show this behaviour. Both protein modifications across all BSM groups have increased cell proliferation rates.

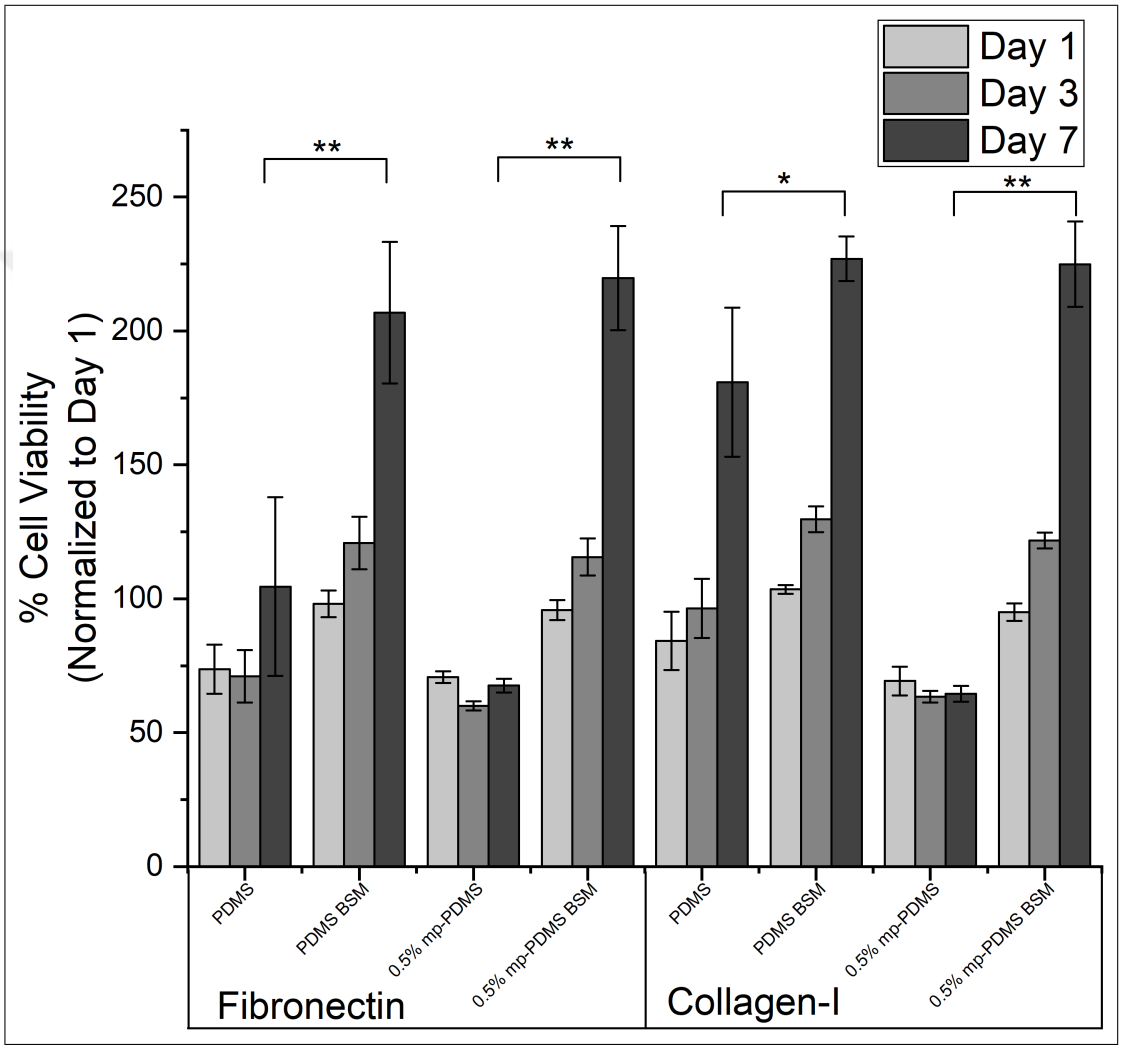

Figure 4.12 alamarBlue cell proliferation assay for PDMS, 0.5% mpPDMS and their BSM variants for different protein coatings (Fibronectin and Col-I). All BSM groups are statistically significant different than their controls. Except for Col-I coated PDMS and BSM PDMS ($p<0.05$), all P-values are smaller than 0.01. (Days 1-7).

4.2.4 Fluorescent Imaging

In order to assess actin cytoskeleton and nuclei localization of osteoblasts adherent on PDMS, 0.5% mpPDMS, BSM PDMS and 0.5% BSM PDMS membranes are given in Figures 4.13 for day 3, 4.14 for day 14 and 4.15 for day 21. Cell morphology and behaviour observed over 21 days in addition to cell viabilities to further assess their cell-cell and cell-surface interactions.

Additionally, actin cytoskeleton and nuclei stainings of adherent cells on uncoated plain PDMS membranes and FN and Col-I coated 0.5% and 1% PDMS membranes were presented as Figure 4.17 and Figure 4.16, respectively, in order to observe cell behaviour morphology on uncoated PDMS membranes and to observe effects of flat 0.5% and 1% PDMS membranes.

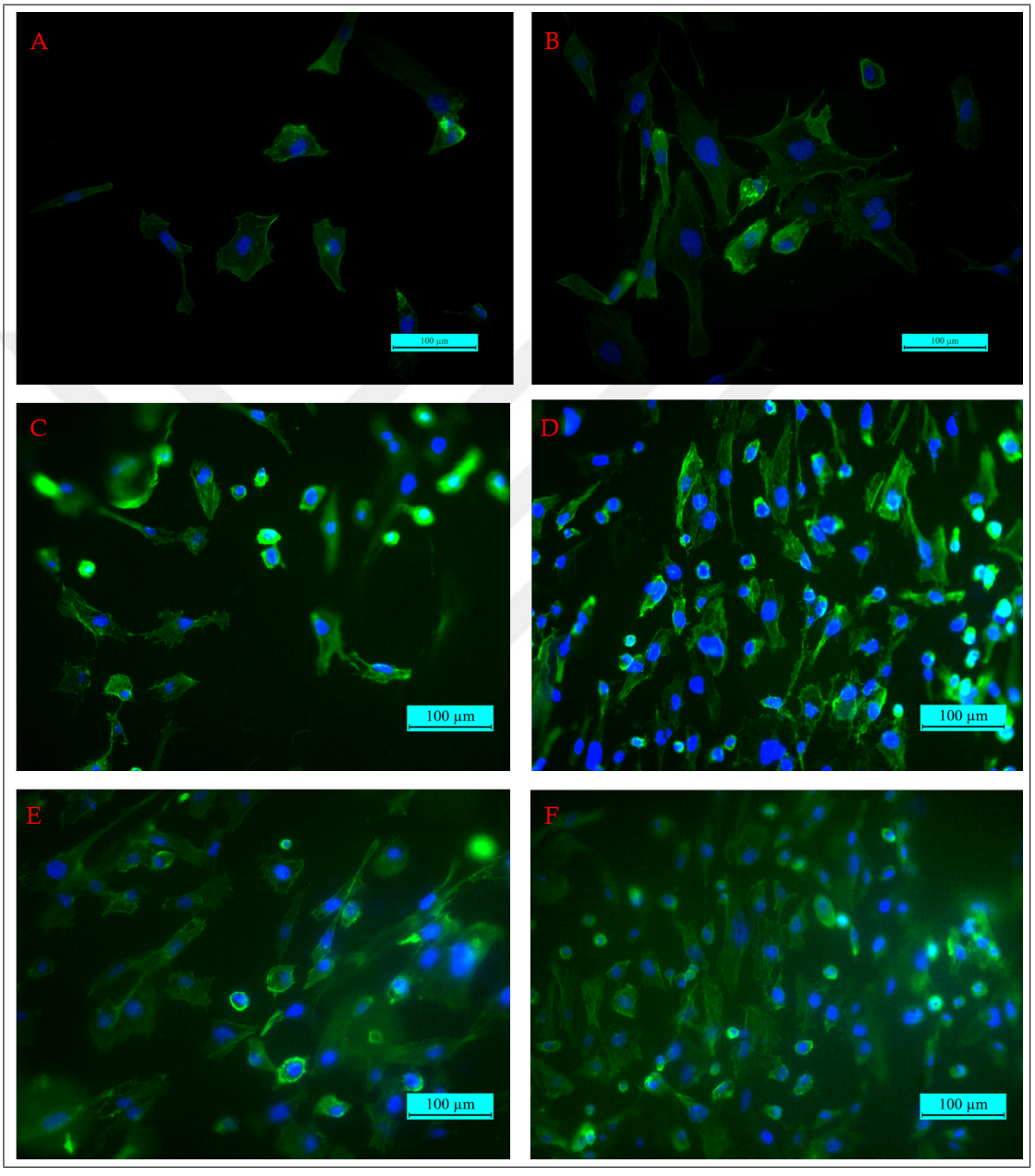

Figure 4.13 Actin filament and nuclei of adherent cells were stained to observe effects of surface topography and protein modifications on cell behaviour and morphology. (A) Plain PDMS+FN, (B) Plain PDMS+Col-I, (C) BSM PDMS+FN, (D) BSM PDMS+Col-I, (E) BSM mpPDMS+FN, (F) BSM mpPDMS+Col-I (Day 3).

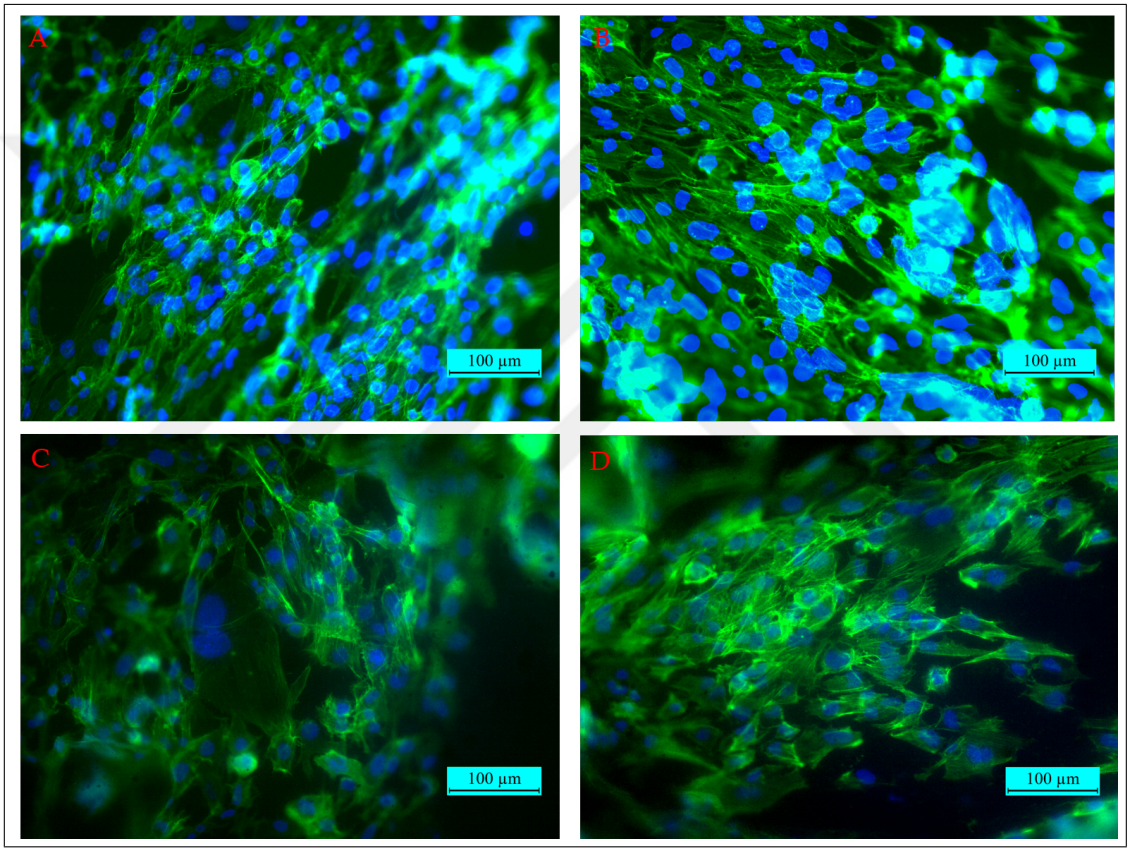

Figure 4.14 Actin filament and nuclei of adherent cells were stained to observe effects of surface topography and protein modifications on cell behaviour and morphology. (A) BSM PDMS+FN, (B) BSM PDMS+Col-I, (C) BSM mpPDMS+FN, (D) BSM mpPDMS+Col-I (Day 14).

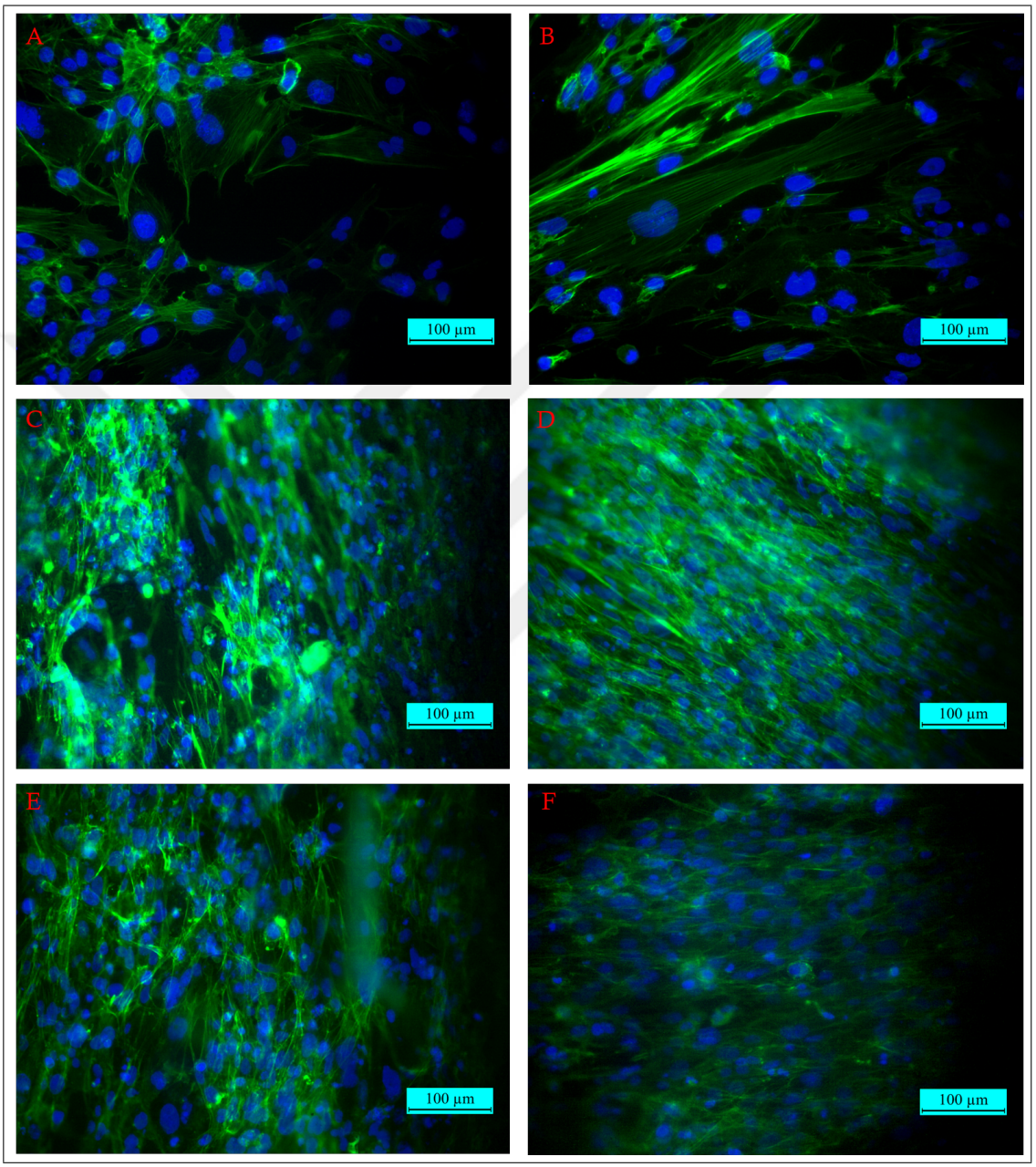

Figure 4.15 Actin filament and nuclei of adherent cells were stained to observe effects of surface topography and protein modifications on cell behaviour and morphology. (A) Plain PDMS+FN, (B) Plain PDMS+Col-I, (C) BSM PDMS+FN, (D) BSM PDMS+Col-I, (E) BSM mpPDMS+FN, (F) BSM mpPDMS+Col-I (Day 21).

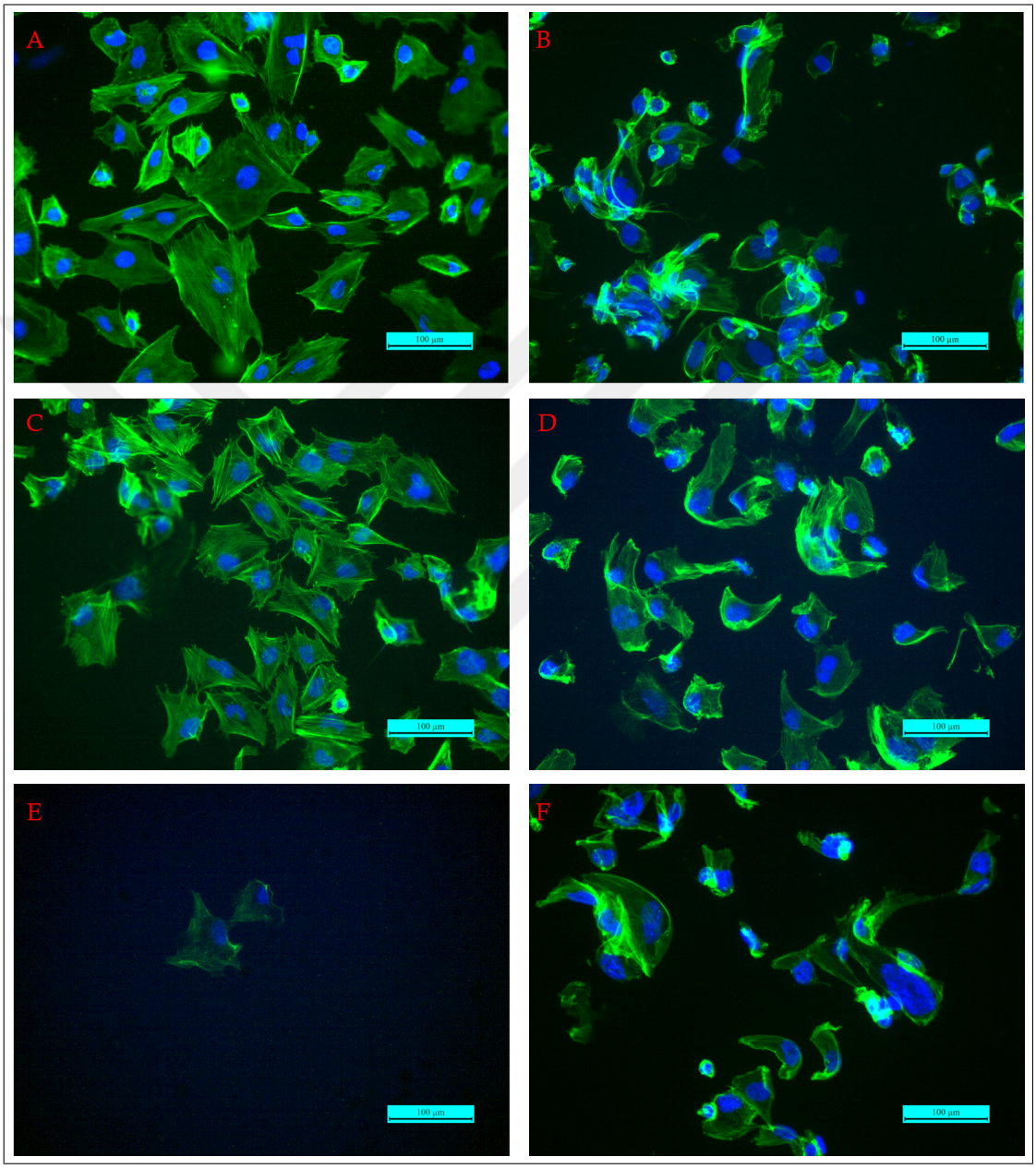

Figure 4.16 Actin filament and nuclei of adherent cells were stained to observe effects magnetic particle presence and protein modifications on cell behaviour and morphology. (A,B) 0.5% mpPDMS+FN, (C,D) 0.5% mpPDMS+Col-I, (E) 1% mpPDMS+FN, (F) 1% mpPDMS+Col-I (Day 7).

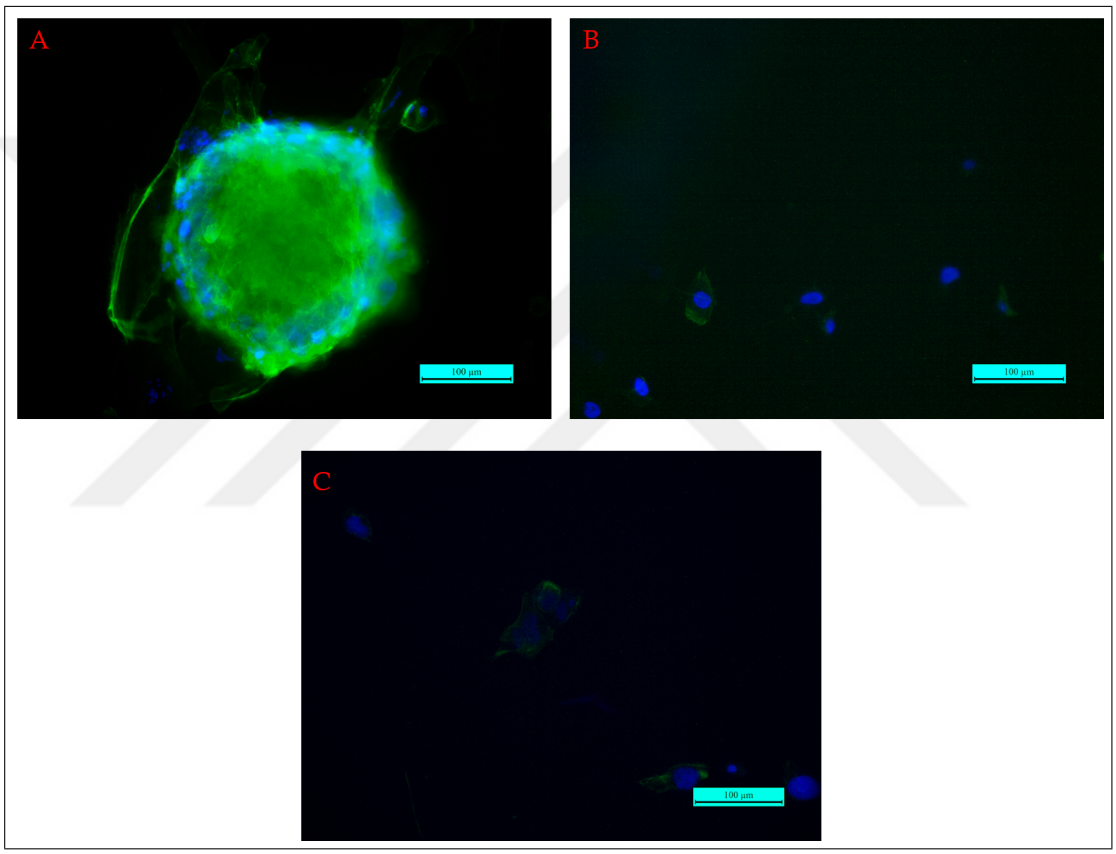

Figure 4.17 Actin filament and nuclei of adherent cells were stained to observe effects of uncoated PDMS surfaces on cell behaviour and morphology. (A) Plain PDMS, (B) 0.5% mpPDMS, (C) 1% mpPDMS (Day 3).

4.3 Statistical Analysis

All statistically significant differences mentioned throughout this thesis were determined using one-way ANOVA with post-hoc Tukey's honest significant difference test where $p<0.05$ was considered to show meaningful statistical difference.

5. DISCUSSION

5.1 Material Characterization

Water contact angle measurements have shown the effect of protein modifications on PDMS membranes. Native PDMS membranes had their signature hydrophobic properties with 104.98 ° [12]. BSM pattern transfer didn't significantly change water wettability properties. Schneider et al. have reported that water contact angle was dependent on geometry of surface properties and not to the height of those properties from material surface [59]. BSM PDMS membranes have high orders of randomness on their surface features and properties,therefore; it is not possible in this case to quantitatively report a water contact angle change depending on the material surface properties alone. This claim is further supported in the literature where the lotus leaves hydrophobic properties are coming from their highly organized and optimized wax crystals and micro scale papillae [60]. On the other hand the protein modified PDMS membranes using O_2 plasma treatment had their water contact angle significantly reduced and shows consistency with works in literature in terms of PDMS surface modifications such as Collagen type IV adsorption [61], C_2F_4 and HEMA modification after O_2 plasma treatment [62], and PEG grafting after O_2 plasma treatment [63]. Collagen-I modified membranes had lower contact angle measurements compared to the ones modified with Fibronectin which was also reported by Kuddannaya et al. [57]. Protein modified BSM PDMS membranes have shown a reverse behaviour on contact angle measurements where the Fibronectin modified membranes yielded smaller contact angle values than the Collagen-I modified membranes. This can be explained with varying surface roughnesses result in different effective surface areas on the membranes. Also as explained above, randomness of surface properties combined with hydrophilized surface might have resulted in this reversed wettability values. Ultimately, protein modification lowered water contact angles of the membranes and positively affected cell viability on those surfaces. Cell adhesion is generally related to surface chemistry and hydrophobicity [64]. In a material characterization point of

view, increased hydrophilicity resulted in cell adhesion on surfaces and enhanced cell proliferation, which will be discussed later in this chapter.

Size distribution of magnetic particles vary from 4 nm to 12 nm with an average of 7.18 nm and standard deviation of 1.95 nm. Mahdavi et al. have shown that the size of the particle change with stirring rate and also points out that stirring rate stops to have an effect on particle size when going past 800rpm. They have also reported that their average particle size and standard deviation as 7.83 nm and 1.87 nm, respectively at 800 rpm stirring rate, which are consistent with our results measured after 1200 rpm mixing rate [65]. Magnetization of magnetic particle embedded PDMS membranes have been measured using VSM. It can be seen that increased concentration of magnetic particles inside membranes also linearly increases magnetization values. Average particle size affect the magnetization values since bulk magnetite (Fe_3O_4) yields 480-500 emu/g of magnetization whereas magnetites of 15 nm in size has shown around 66 emu/g to 68 emu/g of magnetization [66]. Magnetization of the magnetic particles inside polymers has also reported to get weaker because of decreased concentration and also the polymer coating around them [67]. Magnetization curves for 0.5% mpPDMS and 1% mpPDMS membranes reach saturation magnetization at 0.15 emu/g and 0.3 emu/g respectively and both membranes show superparamagnetic behaviour. Increase in magnetization of particles with increased concentration inside the membranes is also consistent with the literature [68].

Transferring bone surface patterns onto PDMS membranes properly and consistently was one of the main challenges to accomplish in order to simulate natural bone microenvironment on a modifiable surface to obtain an effective biomaterial surfaces in terms of topography and optimization of BSM membrane production was crucial. First attempts of BSM PDMS synthesis weren't feasible to be used in cell culture studies due to their thickness. Preliminary studies for this thesis have shown that cells seeded onto thick membranes haven't had enough time to adhere on BSM PDMS surfaces and slipped off of membrane surfaces. Moreover, thicker membranes contain more magnetic particles inside them, rendering their control group inconsistent. To overcome these problems, a method to produce thinner BSM PDMS membranes was developed. Fur-

thermore, BSM PDMS membranes have shown promising pattern transferring quality. When comparing both femur bone and BSM membrane SEM images it can be shown that porous and rough topographical structure is transferred onto PDMS membrane from femur bone. At 2500x magnifications plain PDMS membranes show almost no roughness on the surface, whereas BSM PDMS membrane at the same magnification show greater relative roughness, therefore increased surface area, which is also shown with AFM results and discussed further in AFM section.

Figure 4.3 (A) shows surface topography profile of plain PDMS membrane scanned over 6400 μm^2 area. Surface of plain PDMS membrane was smooth and its roughness was measured in nanometer scale. Figure 4.3 (B) shows surface topography profile for BSM PDMS membrane scanned over 1600 μm^2 area. BSM PDMS membrane has notable differences compared to plain PDMS with surface height changes drastically and its roughness is in micron scale. Surface roughness (S_a) is recorded as 3.0067 nm and root mean square roughness (S_q) is measured as 6.2181 nm for plain PDMS. Recorded values are usually measured between 0.4 nm and 0.65 nm for surface roughness in the literature [69], [70]. Even though measured values for this work are still relatively small compared to BSM experimentation groups (S_a: 223.04 nm and S_q:292.05 nm), it is still almost 5-fold higher than reported values. It might have been caused prolonged periods of curing time due to the fact that all membranes were attached to plate surfaces using same PDMS formulation to avoid any cell to proliferate on tissue culture plates, practically at least doubling the time required the PDMS to cure fully. Types of curing usually do not exceed 75 °C for 4 hours but rarely goes above 100 °C, even so curing times above 100 °C is generally under half an hour for thin films. A reported AFM study cured 2mm of thin PDMS film at 150 °C for only 10 minutes before analysis [70]. Prolonged periods of curing time may have affected the topographical properties by forming nano-scale cracks on the surface.

Chemical compositions of magnetic particle embedded membranes used in this study were investigated using FTIR spectroscopy. Figure 4.7 shows spectra of plain PDMS, and mpPDMS membranes with different magnetic particle concentrations. Characteristic absorption bands for PDMS are clearly visible around wavenumbers

2900, 1450, 1410, 1250 and 1000 cm^{-1}, representing the stretching, rocking and bending of bonds present in its chemical structure in addition to the band around 560 cm^{-1}, a characteristic of Fe-O bonding generated from magnetite present inside the polymer and all spectra are consistent with the literature [71]. Enlarged part of the spectra on Figure 4.7 clarifies the effect of increased magnetic particle concentration. Peak observed around 560 cm^{-1} from the spectra of 1%mpPDMS decreases in strength compared to 0.5%mpPDMS peak, which can be explained by the increased absorption resulted from increased particle concentration. Also to verify protein modification of the membranes, FTIR spectra for PDMS, and PDMS membranes modified with Fibronectin and Collagen-I proteins were separately taken. Peaks around 3345 cm^{-1} is visible for both protein modifications. These peaks are often associated with secondary amine (-NH) bending. Furthermore, protein specific C=O bands are visible around 1636 cm^{-1}. Both of these absorption bands are consistent with literature [72]. Also, a peak around 1537 cm^{-1} is also visible and it is associated with amide II absorption due to the N-H bending and C-N stretch [73]. It can be concluded that the protein modifications along with magnetic particle embedding on PDMS membranes were successful.

5.2 Cell culture studies

Indirect MTT assay conducted in order to assess any possible cytotoxicity may have caused by the presence of magnetic particles inside PDMS membranes haven't shown any cytotoxic effect on cell proliferation. All groups were on par in terms of proliferation. To better focus on the effects of different parameters introduced in this study, some experimental groups listed on Table 4.2 were eliminated using cell viability data presented in Figure 4.10 and Figure 4.11. Cell viability on protein coated membranes have shown significant differences over uncoated membranes. Inefficiency and negative effects of plain PDMS membrane on cell growth is reported in the literature [74]. However Collagen-I and Fibronectin coated membranes overcame this problem by creating a surface with ECM proteins where integrin receptors can attach to them. Even though it is reported in the literature that the Fibronectin coatings are superior

to the other ECM molecules in terms of cell adhesion and spreading [75], Collagen coatings on these membranes has shown better viability results in this study, but they are not significantly different. It may be concluded that, cellular viability is less dependent on initial cell adhesion in case of PDMS membranes. It should be also noted that there are several other parameters such as the effects of magnetic particles and mechanical properties that may have played a role on this behaviour. Experiment presented in Figure 4.11 was conducted to assess the effect of magnetic fields on cell proliferation among plain and BSM groups. Cells seeded on BSM membranes have shown an increasing trend across all experimental groups and their % cell viabilities (normalized to TCP) were significantly different compared to their plain control groups ($p<0.01$). Overall, there is no statistical significant differences of cellular viability between magnetic field and non-magnetic field groups. On both main groups (Magnetic Field and Control (Non-magnetic field), cells have shown a decreasing trend of cell viability on 1% mpPDMS membranes. 0.5% mpPDMS groups and plain PDMS membranes were relatively static in terms of cell viability. Difference between the data presented on Figure 4.10 and Figure 4.11 is the cell seeding density. Former of these two has generated from a cell seeding amount of 25000 per well, whereas latter of these two has been generated from a cell seeding amount of 15000 per well. It has been reported on the literature that cell proliferation rates are effected from cell seeding density [76]. It may be concluded that the initial amount of cells per well effected cell proliferation. On spite of these results, to make the study to focus more on bone surface mimicry and effects of magnetic particle presence on osteoblast cell metabolism, static magnetic field groups along with 1% mpPDMS groups are completely removed from the study. Also, increased magnetic particle concentration on PDMS membranes gets increasingly difficult to homogenize, visible clearly on the surface imperfections, therefore changing the surface roughness, on 2% mpPDMS membrane in Figure 3.4, which has been proven to be another factor to include well-suited control groups to the study.

Cell viability data was obtained using alamarBlue cell proliferation assay to observe metabolic activity on plain and BSM PDMS membranes. All membranes were coated with either type-I Collagen or Fibronectin to mimic ECM microenvironment on a molecular level. These two proteins are available in natural bone matrix along with

noncollagenous proteins such as osteocalcin, osteopontin ans osteonectin [28]. Previous attempts to mimic natural bone microenvironment that only consisted of topographical mimicry without any protein modification yielded low levels of cell attachment and proliferation. Figures 4.12 show cell proliferation on experimental groups with FN and Col-I surface modifications. Bone surface pattern transfer onto PDMS membranes increased osteoblast cell proliferation across all experimental groups compared to their plain counterparts ($p<0.01$). Only exception is Col-I coated PDMS to its BSM counterpart that has a slightly higher p-value ($p<0.05$). Correlation between surface roughness and cell adhesion has been reported in the literature for different types of scaffolding materials on cell lines such as fibroblasts [77], and osteoblasts [78], [79]. Even though plain PDMS membranes coated with either protein continue to have increased proliferation potential, fibronectin coated plain PDMS membranes had a lesser rate of increase compared to its Collagen coated counterpart. This can be explained by the abundance of collagenous proteins naturally available at bone matrix. Therefore Col-I coating, along with BSM surfaces, provided osteoblasts to proliferate under more natural microenvironment. It should be noted that abundance of collagen resulted in relatively better results comparing Plain PDMS+FN and Plain PDMS+Col-I, it is reported in the literature proteins containing RGD sites, such as fibronectin, are needed initiate particular pathways of bone formation [80]. Cells adherent on membrane surfaces coated with collagen may have resulted in better viabilities but it can be argued that several pathways would not be activated until cells secrete their own ECM, which may ultimately yield the same results with the cells initially adhered on Fibronectin in the long run. Plain mpPDMS membranes have shown very little proliferation. On the contrary, BSM mpPDMS membranes have shown the similar rates of proliferation as BSM PDMS membranes, whereas plain PDMS membranes without magnetic particles didn't show such variety compared to BSM PDMS membranes and proliferation has been observed on plain membranes with both protein modifications. Effect of surface topography on osteoblastic growth and differentiation is shown to be an enhancing feature in the literature[81], [82]. However, there is no reported evidence of how magnetic particles effect cell metabolism on plain membranes to our knowledge. This phenomena could be explained with several propositions. It is reported in the literature that magnetic nanoparticle embedded scaffolds upregulated integrin subsets $\alpha 1$,$\alpha 2$,$\beta 1$,$\beta 3$

and also it is reported that $\alpha 1\beta 1$ and $\alpha 2\beta 1$ integrins are specific to collagen binding whereas $\alpha V\beta 3$ integrin is specific to RGD sequenced proteins such as fibronectin. It is also reported that the mechanotransductive pathways are initiated through integrin binding sites [83]. It may be speculated that the possibility of increased integrin regulation resulted in some mechanotransduction related signaling events and resulted in decrease or stasis in proliferation. Another possibility of this proliferation profile may have caused by surface stiffness. It is also known that the surface stiffness affect cell proliferation [84]. Addition of magnetic particles inside PDMS membranes ultimately change the composition of the polymeric structure; therefore, changing stiffness of the membrane. Stiffness changes also affect mechanotransduction, such as Rho/ROCK signalling pathways [85], which are responsible for motility, cellular contraction, cell division and morphology [86].

Overall, results obtained from alamarBlue cell proliferation assay can also be interpreted as the effect of surface topography on cell adhesion and growth overcomes the inhibition effect thought to be originated from embedded magnetic particles.

To evaluate osteoblast behavior and growth patterns on all PDMS membranes and visualize actin cytoskeleton and nuclei, adherent cells were stained with phalloidin for F-actin and DAPI for nucleus. Imaging of actin filaments and nuclei at day 3 have shown how surface topography and chemistry affected osteoblast cell adhesion. Figure 4.17 shows cell behavior on uncoated PDMS membranes. Osteoblast cells minimized their surface interactions by forming a cell sphere. It is known that surface hydrophobicity decreases cell adhesion [64]. As reported in Table 4.1, plain PDMS membranes are hydrophobic. By contacting more with neighboring cells, they have minimized their surface interactions with PDMS. (B) and (C) also show minimal cell-surface interactions with surroundings for 0.5% and %1 mpPDMS membranes, respectively and adherent cell amount was significantly decreased. This lower amount of adherent cells have also been observed in cell viability studies in Figure 4.10. Figure 4.13(A) shows cell adhesion behavior on plain PDMS membranes with FN coating, the cells remain disconnected from each other, whereas, (B) shows the behavior on its Col-I coated counterpart. Cells started to stretch and they began to interact with surface and each

other by their filopodia, trying to communicate and migrate. BSM surfaces provided a better environment for cell adhesion and growth. Fibronectin coated membranes BSM PDMS membranes(C) shows similar filopodia behavior as (B) and Collagen coated membranes started to show pattern adaptation and began to align in a unidirectional fashion. Filopedia are still present to find desirable migration paths. Same conclusions of filopodia presence can be made on BSM mpPDMS, (E) and (F), but as discussed before, presence of magnetic particles somehow inhibit cell growth and this phenomena is present on some cells which they preferred to minimize contact area with the surface even on more suitable Col-I coating whereas some cells have shown the same behaviour as BSM membranes.

Staining of day 14 samples have shown more organized patterns of cell formation on each BSM membrane. Most of the surfaces of these membranes were covered with cells at this point and cells started to show contact inhibition some point closely before or just after day 14 which was observed during cell proliferation studies. Images taken from this day forward was taken near the edges of cell mono layers to investigate better filament organization(Figure 4.14). All the adherent cell on membranes created their ECM at this point. Fibronectin coated BSM PDMS membranes (A) build their actin filament network more randomly at moderate levels compared to Collagen coated BSM membranes(B). It is still challenging to find distinguishing differences between two different protein coatings after they reach confluency. It is known that the osteoblasts interact and adhere to surfaces using integrins present on their membrane to the proteins bound to membrane surface initially, after secretion of ECM proteins these cells also interact with new proteins present in the environment [79]. Figure 4.14(C) and (D) shows cell behavior on BSM mpPDMS with FN and Col-I modifications, respectively. Effect of magnetic particles are still present, where some cells do not show classic osteoblastic morphology and smaller in size with more randomized actin filament organization. On the other hand, cell proliferation on BSM mpPDMS membranes are on par with BSM PDMS membranes. It can be argued that different cellular morphologies might show similar cell proliferation.

Figure 4.15(A) and (B), which are plain PDMS membranes coated with FN

and Col-I respectively, show differences in cellular alignment. Even without the rough pattern provided by BSM membranes, Col-I coated cells exhibit a clear tendency to unidirectional alignment with actin filaments few hundred microns long where cells adherent on the FN coated membranes preferred more random placement and tend to clump together. It is reported in the literature that cell follow the alignment of Collagen-I secreted for ECM [87]. BSM membranes of same day (C) and (D) also exhibit the same directional pattern same as their controls. FN coated BSM membrane demonstrate more clumping and formation of more randomized actin network with nuclei generally inclined to stay together. Col-I coated membranes continued to form more unidirectionally aligned actin network. This stretching behaviour on both coated membranes may have resulted in different signalling pathways such as Runx2, ALP, Osterix (OSX) and Osteocalcin (OCN) as reported in the literature [88], and it is also discussed as a precursor events for osteoblast differentiation to osteocytes [28]. After 21 days of incubation, differentiation is expected. It is clear that surface roughness of BSM PDMS and 0.5% BSM mpPDMS membranes assisted osteoblasts to show significantly increased cell proliferation and natural cell morphology but without quantifying gene expression profiles for these pathways on these stages it is not possible to reach to certain conclusions about differentiation.

In order to assess the effects mpPDMS membranes with increasing concentrations of embedded magnetic particles on adherent cells, another actin cytoskeleton/nuclei staining was performed after BSM actin cytoskeleton/nuclei staining, using the method given in Section 3.6.3. Figure 4.16 (A,B) shows cell morphology on different sites on FN coated 0.5% mpPDMS membranes. (A) shows a natural osteoblastic morphology, whereas, (B) shows a crescent shaped morphology. Even though both images were taken from the same membrane, cellular morphology changes throughout the membrane. Same trend continues with Col-I coated %0.5 mpPDMS membranes (C) and (D). Finally (E) and (F), which are adherent cells on %1 mpPDMS+FN and 1% mpPDMS+Col-I, show decreased amount of adherent cells on those membranes. Crescent shaped cells were still present on Col-I coated membranes, but FN coated %1 mpPDMS membranes lost almost all their adherent cells. All stainings are consistent with our cell viability results. Even though magnetic particles were dispersed

homogeneously, these particles tend to agglomerate and form clusters during degassing process, resulting in increased concentration of magnetic particles in some sites of membranes. This crescent shape behavior can be associated with cellular migration, where F-actin filaments were recruited to the adhesion sites [83]. On images (B, D and F) increased actin signals can be observed on migration front, usually towards the same direction. Movement of cells also create traction force underneath the cell which regulates mechanotransduction processes [29]. It is also reported in the literature that the shear stress applied onto osteoblast cells trigger intracellular pathways related with focal adhesions [89]. It might be speculated that this mechanotransductive effects resulted from magnetic particle presence affect cell adhesion and migration. Especially on 1% mpPDMS membranes, adherent cells may have constantly tried to migrated and weren't able to form cell-cell interactions through N-Cadherins, which was reported to be an important factor for elaboration of a osteoblastic morphology [90]. On the contrary, the reason BSM mpPDMS membranes did not show this kind of behavior can be explained as the effect of surface patterning and roughness, which is also reported to be a factor in cellular movement [91], which may have resulted in more efficient migration and finding a location for suitable proliferation sites. All these effects combined might explain as how magnetic particle presence in PDMS membranes affect cell migration and proliferation in terms of cell viability and morphology, but the results obtained from cell viability and stainings of 0.5% and 1% mpPDMS membranes differ significantly; therefore, more detailed studies should be carried out in terms of gene expressions responsible for focal adhesions, integrins, and proliferation related markers to further understand how magnetic particle presence effects osteoblast cell behavior.

5.3 Conclusion

In conclusion, variants of PDMS membranes,bone surface mimicked, magnetic particle embedded, and combination of both, were successfully produced and has proven to be usable in osteoblast cell culture studies. Pattern transfer onto BSM membranes were also which was shown successful shown with SEM and AFM. Easily replicable homogeneous dispersion of magnetic particles in a polymer as viscous as PDMS was

also achieved, which was a first in this field to our knowledge. Evidence gathered from cellular characterizations, BSM membranes significantly enhanced cell functionality investigated in this thesis such as, increased cell viability, natural morphology and ECM secretion. Different types of protein modifications were investigated in this study and it was concluded that the both protein modifications are viable for cell growth and metabolic activities, Col-I modifications have shown to be better candidates for early growth phases on both plain and BSM PDMS membranes, mainly because their abundance and presence in natural bone microenvironment. Effects of magnetic particles were also investigated but more studies should be conducted to make a more detailed conclusion on the effects of magnetic particles on cell viability and morphology. Effect of surface topography of BSM PDMS membranes overcame the effect of magnetic fields on cell proliferation and extraordinarily increased viability to the level of plain BSM PDMS membrane groups. Collective evidence from this study also suggests that the magnetic particle presence in membranes affect cellular migration and sensing functions via mechanotransductive pathways.

5.4 Future studies

To further investigate possible effects of these particles, expressions of osteoblast specific and possible magnetic field related genes will be examined after extensively reviewing the current literature. Also stiffness is another important factor in mechanosensing and all the work done for this thesis conducted with a constant material stiffness. Better candidates for optimized stiffness will be investigated and would be implemented to future studies.

APPENDIX A. SUPPLEMENTARY INFORMATION

A.1 Bradford Protein Quantification Assay

Protein content in Collagen-I solutions were quantified using Bradford Protein Quantification Assay. 2 mg/mL of BSA in dH_2O was prepared and a protein standards were diluted from that solution, ranging from 1500 μg/mL to 125 μg/mL with 250 μg/mL increments. 250 μL of Coomassie Brilliant Blue was added to each well along with 5 μL of each standard or protein solution. Absorbances were measured at 595 nm and 450 nm and their ratio was plotted against concentrations to obtain a calibration curve. Collagen-I concentration inside the protein solution were calculated using the calibration curve prepared using BSA standards.

Solubility of type I collagen purified from rat tails were analyzed using Bradford protein quantification assay as reported previously [92]. Using the calibration curve given in appendix section Figure A.2, Collagen-I dissolved in 0.5M acetic acid solution was 40.89 μg/mL. Using the calibration curve given in appendix section Figure A.1, Collagen-I dissolved in 0.1M acetic acid solution was 26.97 μg/mL.

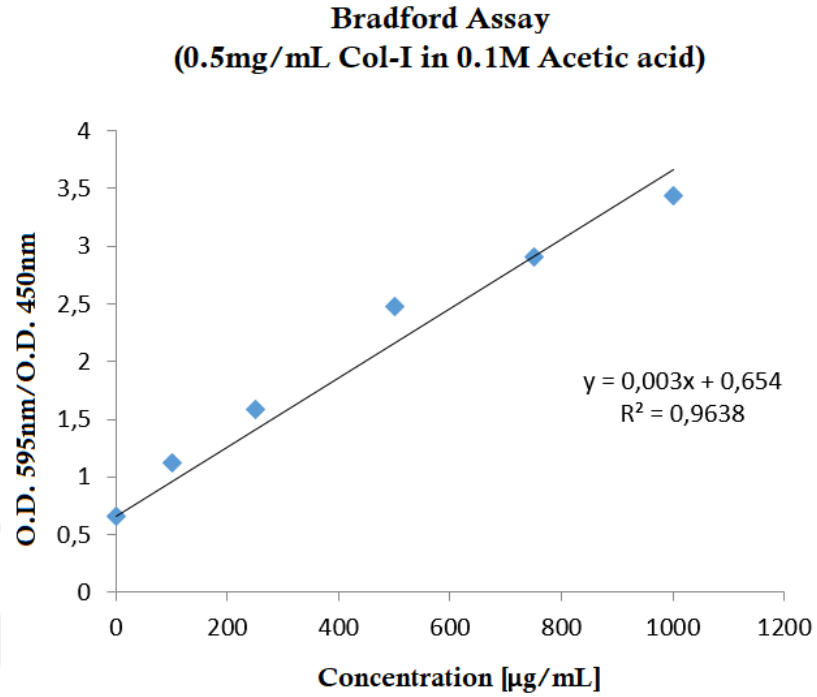

Figure A.1 Calibration curve for Bradford assay created for 0.1M Acetic acid solubility.

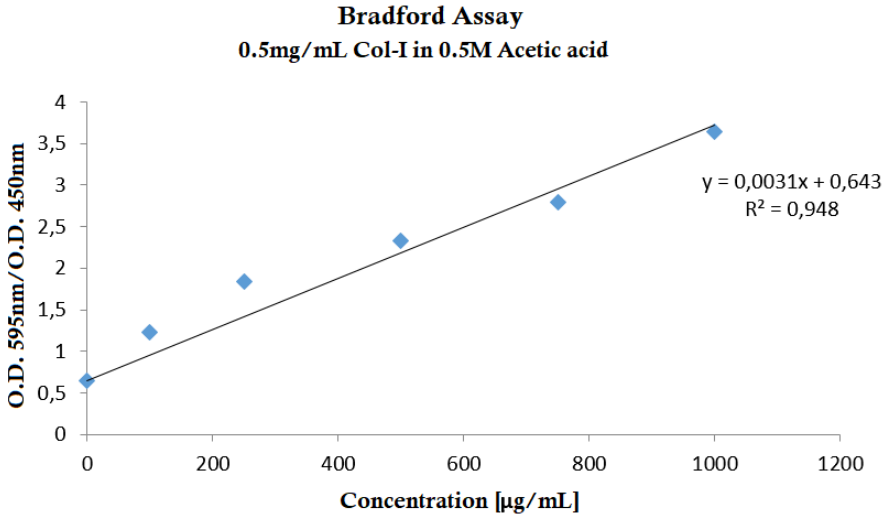

Figure A.2 Calibration curve for Bradford assay created for 0.5M Acetic acid solubility.

Calibration curves for protein concentrations for both 0.1M and 0.5M acetic acid solvents are given above.

REFERENCES

1. Dimitriou, R., E. Jones, D. McGonagle, and P. V. Giannoudis, "Bone regeneration: current concepts and future directions," *BMC Medicine*, Vol. 9, p. 66, 12 2011.

2. Dang, M., L. Saunders, X. Niu, Y. Fan, and P. X. Ma, "Biomimetic delivery of signals for bone tissue engineering," *Bone Research*, Vol. 6, no. 1, 2018.

3. Ozcelik, H., M. Hindie, A. Hasan, N. Engin, V. Cell, J. Barthes, H. Özçelik, M. Hindié, A. Ndreu-halili, and N. E. Vrana, "Cell Microenvironment Engineering and Monitoring for Tissue Engineering and Regenerative Medicine : The Citation Accessed Citable Link Cell Microenvironment Engineering and Monitoring for Tissue Engineering and Regenerative Medicine : The Recent Advances," *BioMed Research International*, Vol. 2014, no. i, p. 18, 2014.

4. Shakiba, D., B. Babaei, F. Saadat, S. Thomopoulos, and G. M. Genin, "The fibrous cellular microenvironment, and how cells make sense of a tangled web," *Proceedings of the National Academy of Sciences*, Vol. 114, no. 23, pp. 5772–5774, 2017.

5. Martino, F., A. R. Perestrelo, V. Vinarský, S. Pagliari, and G. Forte, "Cellular mechanotransduction: From tension to function," *Frontiers in Physiology*, Vol. 9, no. JUL, pp. 1–21, 2018.

6. Stevens, M. M., "Biomaterials for bone tissue engineering," *Materials Today*, Vol. 11, pp. 18–25, 5 2008.

7. Dalby, M. J., N. Gadegaard, R. Tare, A. Andar, M. O. Riehle, P. Herzyk, C. D. Wilkinson, and R. O. Oreffo, "The control of human mesenchymal cell differentiation using nanoscale symmetry and disorder," *Nature Materials*, Vol. 6, no. 12, pp. 997–1003, 2007.

8. Thibault, R. A., A. G. Mikos, and F. K. Kasper, "Scaffold/Extracellular Matrix Hybrid Constructs for Bone-Tissue Engineering," *Advanced Healthcare Materials*, Vol. 2, pp. 13–24, 1 2013.

9. Pedraza, E., A.-C. Brady, C. A. Fraker, and C. L. Stabler, "Synthesis of macroporous poly(dimethylsiloxane) scaffolds for tissue engineering applications," *Journal of Biomaterials Science, Polymer Edition*, Vol. 24, pp. 1041–1056, 6 2013.

10. Jiang, Y., H. Wang, S. Li, and W. Wen, "Applications of Micro/Nanoparticles in Microfluidic Sensors: A Review," *Sensors*, Vol. 14, pp. 6952–6964, 4 2014.

11. Wolf, M. P., G. B. Salieb-Beugelaar, and P. Hunziker, "PDMS with designer functionalities-Properties, modifications strategies, and applications," *Progress in Polymer Science*, Vol. 83, pp. 97–134, 2018.

12. Gokaltun, A., M. L. Yarmush, A. Asatekin, and O. B. Usta, "Recent advances in nonbiofouling PDMS surface modification strategies applicable to microfluidic technology," *Technology*, Vol. 05, no. 01, pp. 1–12, 2017.

13. Gale, B., A. Jafek, C. Lambert, B. Goenner, H. Moghimifam, U. Nze, and S. Kamarapu, "A Review of Current Methods in Microfluidic Device Fabrication and Future Commercialization Prospects," *Inventions*, Vol. 3, no. 3, p. 60, 2018.

14. Yun, H. M., S. J. Ahn, K. R. Park, M. J. Kim, J. J. Kim, G. Z. Jin, H. W. Kim, and E. C. Kim, *Magnetic nanocomposite scaffolds combined with static magnetic field in the stimulation of osteoblastic differentiation and bone formation*, Vol. 85, Elsevier Ltd, 2016.

15. Clarke, B., "Normal Bone Anatomy and Physiology," *Clinical Journal of the American Society of Nephrology*, Vol. 3, pp. S131–S139, 11 2008.

16. Downey, P. A., and M. I. Siegel, "Bone Biology and the Clinical," *Journal of Physical Therapy*, Vol. 86, no. 1, pp. 77–91, 2006.

17. Ott, S. M., "Cortical or Trabecular Bone: What's the Difference?," *American Journal of Nephrology*, Vol. 47, no. 6, pp. 373–375, 2018.

18. Oftadeh, R., M. Perez-Viloria, J. C. Villa-Camacho, A. Vaziri, and A. Nazarian, "Biomechanics and Mechanobiology of Trabecular Bone: A Review," *Journal of Biomechanical Engineering*, Vol. 137, no. 1, p. 010802, 2015.

19. Weatherholt, A. M., R. K. Fuchs, and S. J. Warden, "Specialized connective tissue: Bone, the structural framework of the upper extremity," *Journal of Hand Therapy*, Vol. 25, no. 2, pp. 123–132, 2012.

20. Dwek, J. R., "The periosteum: what is it, where is it, and what mimics it in its absence?," *Skeletal Radiology*, Vol. 39, no. 4, pp. 319–323, 2010.

21. Mahajan, A., "Periosteum: A highly underrated tool in dentistry," *International Journal of Dentistry*, Vol. 2012, no. Figure 2, 2012.

22. Berendsen, A. D., and B. R. Olsen, "Bone development," *Bone*, Vol. 80, pp. 14–18, 11 2015.

23. Syed-Picard, F. N., G. A. Shah, B. J. Costello, and C. Sfeir, "Regeneration of periosteum by human bone marrow stromal cell sheets," *Journal of Oral and Maxillofacial Surgery*, Vol. 72, no. 6, pp. 1078–1083, 2014.

24. Lerner, U. H., "Osteoblasts, Osteoclasts, and Osteocytes: Unveiling Their Intimate-Associated Responses to Applied Orthodontic Forces," *Seminars in Orthodontics*, Vol. 18, no. 4, pp. 237–248, 2012.

25. Compton, J. T., and F. Y. Lee, "A Review of Osteocyte Function and the Emerging Importance of Sclerostin," *The Journal of Bone and Joint Surgery-American Volume*, Vol. 96, pp. 1659–1668, 10 2014.

26. Dallas, S. L., M. Prideaux, and L. F. Bonewald, "The Osteocyte: An Endocrine Cell and More," *Endocrine Reviews*, Vol. 34, pp. 658–690, 10 2013.

27. Raisz, L. G., "Physiology and pathophysiology of bone remodeling," *Clinical Chemistry*, Vol. 45, no. 8 II, pp. 1353–1358, 1999.

28. Florencio-Silva, R., G. R. d. S. Sasso, E. Sasso-Cerri, M. J. Simoes, and P. S. Cerri, "Biology of Bone Tissue: Structure, Function, and Factors That Influence Bone Cells," *BioMed Research International*, Vol. 2015, pp. 1–17, 2015.

29. Dong, Y., G. Jin, Y. Hong, H. Zhu, T. J. Lu, F. Xu, D. Bai, and M. Lin, "Engineering the Cell Microenvironment Using Novel Photoresponsive Hydrogels," *ACS Applied Materials and Interfaces*, Vol. 10, no. 15, pp. 12374–12389, 2018.

30. Williams, C. A., and E. B. Lavik, "Engineering the CNS stem cell microenvironment," *Regenerative Medicine*, Vol. 4, no. 6, pp. 865–877, 2009.

31. Hao, Z., Z. Song, J. Huang, K. Huang, A. Panetta, Z. Gu, and J. Wu, "The scaffold microenvironment for stem cell based bone tissue engineering," *Biomaterials Science*, Vol. 5, no. 8, pp. 1382–1392, 2017.

32. Chocholata, P., V. Kulda, and V. Babuska, "Fabrication of Scaffolds for Bone-Tissue Regeneration," *Materials*, Vol. 12, no. 4, p. 568, 2019.

33. Lee, E. J., F. K. Kasper, and A. G. Mikos, "Biomaterials for Tissue Engineering," *Annals of Biomedical Engineering*, Vol. 42, pp. 323–337, 2 2014.

34. Seol, Y.-J., J. Y. Park, J. W. Jung, J. Jang, R. Girdhari, S. W. Kim, and D.-W. Cho, "Improvement of Bone Regeneration Capability of Ceramic Scaffolds by Accelerated Release of Their Calcium Ions," *Tissue Engineering Part A*, Vol. 20, no. 21-22, pp. 2840–2849, 2014.

35. Kroeze, R., M. Helder, L. Govaert, and T. Smit, "Biodegradable Polymers in Bone Tissue Engineering," *Materials*, Vol. 2, pp. 833–856, 7 2009.

36. Liu, X., and P. X. Ma, "Polymeric Scaffolds for Bone Tissue Engineering," *Annals of Biomedical Engineering*, Vol. 32, pp. 477–486, 3 2004.

37. Ghassemi, T., A. Shahroodi, M. H. Ebrahimzadeh, A. Mousavian, J. Movaffagh, and A. Moradi, "Current Concepts in Scaffolding for Bone Tissue Engineering," *The Archives of Bone and Joint Surgery*, Vol. 6, pp. 90–99, 3 2018.

38. Chuah, Y. J., Y. T. Koh, K. Lim, N. V. Menon, Y. Wu, and Y. Kang, "Simple surface engineering of polydimethylsiloxane with polydopamine for stabilized mesenchymal stem cell adhesion and multipotency," *Scientific Reports*, Vol. 5, no. November, pp. 1–12, 2015.

39. Trantidou, T., Y. Elani, E. Parsons, and O. Ces, "Hydrophilic surface modification of pdms for droplet microfluidics using a simple, quick, and robust method via pva deposition," *Microsystems and Nanoengineering*, Vol. 3, no. April 2016, 2017.

40. Sia, S. K., and G. M. Whitesides, "Microfluidic devices fabricated in poly(dimethylsiloxane) for biological studies," *Electrophoresis*, Vol. 24, no. 21, pp. 3563–3576, 2003.

41. Velve-Casquillas, G., M. Le Berre, M. Piel, and P. T. Tran, "Microfluidic tools for cell biological research," *Nano Today*, Vol. 5, pp. 28–47, 2 2010.

42. Schneemilch, M., and N. Quirke, "Effect of oxidation on the wettability of poly(dimethylsiloxane) surfaces," *Journal of Chemical Physics*, Vol. 127, no. 11, pp. 1–8, 2007.

43. Fan, F. R., J. Luo, W. Tang, C. Li, C. Zhang, Z. Tian, and Z. L. Wang, "Highly transparent and flexible triboelectric nanogenerators: Performance improvements and fundamental mechanisms," *Journal of Materials Chemistry A*, Vol. 2, no. 33, pp. 13219–13225, 2014.

44. Hillborg, H., and U. Gedde, "Hydrophobicity recovery of polydimethylsiloxane after exposure to corona discharges," *Polymer*, Vol. 39, pp. 1991–1998, 5 1998.

45. Tan, S. H., N.-T. Nguyen, Y. C. Chua, and T. G. Kang, "Oxygen plasma treatment for reducing hydrophobicity of a sealed polydimethylsiloxane microchannel," *Biomicrofluidics*, Vol. 4, p. 032204, 9 2010.

46. Almutairi, Z., C. L. Ren, and L. Simon, "Evaluation of polydimethylsiloxane (PDMS) surface modification approaches for microfluidic applications," *Colloids and Surfaces A: Physicochemical and Engineering Aspects*, Vol. 415, pp. 406–412, 2012.

47. Shuwen Hu, Xueqin Ren, Mark Bachman, Christopher E. Sims, G. P. Li, and Nancy Allbritton, "Surface Modification of Poly(dimethylsiloxane) Microfluidic Devices by Ultraviolet Polymer Grafting," *Analytical chemistry*, Vol. 74, no. 16, pp. 4117–4123, 2002.

48. Saunders, R., "Static magnetic fields: Animal studies," *Progress in Biophysics and Molecular Biology*, Vol. 87, no. 2-3 SPEC. ISS., pp. 225–239, 2005.

49. Kim, E. C., J. Park, I. K. Kwon, S. W. Lee, S. J. Park, and S. J. Ahn, "Static magnetic fields promote osteoblastic/cementoblastic differentiation in osteoblasts, cementoblasts, and periodontal ligament cells," *Journal of Periodontal and Implant Science*, Vol. 47, no. 5, pp. 273–291, 2017.

50. Wiskirchen, J., E. F. Groenewaeller, R. Kehlbach, F. Heinzelmann, M. Wittau, H. P. Rodemann, C. D. Claussen, and S. H. Duda, "Long-term effects of repetitive exposure to a static magnetic field (1.5 T) on proliferation of human fetal lung fibroblasts," *Magnetic Resonance in Medicine*, Vol. 41, no. 3, pp. 464–468, 1999.

51. Pacini, S., M. Gulisano, B. Peruzzi, E. Sgambati, G. Gheri, S. G. Bryk, S. Vannucchi, G. Polli, and M. Ruggiero, "Effects of 0.2 T static magnetic field on human skin fibroblasts," *Cancer Detection and Prevention*, Vol. 27, no. 5, pp. 327–332, 2003.

52. Tsai, M. T., W. H. S. Chang, K. Chang, R. J. Hou, and T. W. Wu, "Pulsed electromagnetic fields affect osteoblast proliferation and differentiation in bone tissue engineering," *Bioelectromagnetics*, Vol. 28, no. 7, pp. 519–528, 2007.

53. Su, C.-Y., T. Fang, and H.-W. Fang, "Effects of Electrostatic Field on Osteoblast Cells for Bone Regeneration Applications," *BioMed Research International*, Vol. 2017, pp. 1–9, 2017.

54. Qian, A. R., X. Gao, W. Zhang, J. B. Li, Y. Wang, S. M. Di, L. F. Hu, and P. Shang, "Large Gradient High Magnetic Fields Affect Osteoblast Ultrastructure and Function by Disrupting Collagen I or Fibronectin/$\alpha\beta$1 Integrin," *PLoS ONE*, Vol. 8, no. 1, 2013.

55. Cunha, C., S. Panseri, M. Marcacci, and A. Tampieri, "Evaluation of the Effects of a Moderate Intensity Static Magnetic Field Application on Human Osteoblast-Like Cells," *American Journal of Biomedical Engineering*, Vol. 2, pp. 263–268, 1 2013.

56. Demir, Ö., "Bone Surface Mimicked Biodegradable Polymeric Scaffolds," Master's thesis, Boğaziçi University, 2014.

57. Kuddannaya, S., Y. J. Chuah, M. H. A. Lee, N. V. Menon, Y. Kang, and Y. Zhang, "Surface Chemical Modification of Poly(dimethylsiloxane) for the Enhanced Adhesion and Proliferation of Mesenchymal Stem Cells," *ACS Applied Materials & Interfaces*, Vol. 5, pp. 9777–9784, 10 2013.

58. Waiwijit, U., T. Maturos, S. Pakapongpan, D. Phokharatkul, A. Wisitsoraat, and A. Tuantranont, "Highly cytocompatible and flexible three-dimensional graphene/polydimethylsiloxane composite for culture and electrochemical detection of L929 fibroblast cells," *Journal of Biomaterials Applications*, Vol. 31, no. 2, pp. 230–240, 2016.

59. Schneider, L., M. Laustsen, N. Mandsberg, and R. Taboryski, "The Influence of Structure Heights and Opening Angles of Micro-and Nanocones on the Macroscopic Surface Wetting Properties," *Scientific Reports*, Vol. 6, no. September 2015, pp. 1–9, 2016.

60. Ensikat, H. J., P. Ditsche-Kuru, C. Neinhuis, and W. Barthlott, "Superhydrophobicity in perfection: The outstanding properties of the lotus leaf," *Beilstein Journal of Nanotechnology*, Vol. 2, no. 1, pp. 152–161, 2011.

61. Palchesko, R. N., L. Zhang, Y. Sun, and A. W. Feinberg, "Development of Polydimethylsiloxane Substrates with Tunable Elastic Modulus to Study Cell Mechanobiology in Muscle and Nerve," *PLoS ONE*, Vol. 7, no. 12, 2012.

62. Bodas, D., and C. Khan-Malek, "Formation of more stable hydrophilic surfaces of PDMS by plasma and chemical treatments," *Microelectronic Engineering*, Vol. 83, no. 4-9 SPEC. ISS., pp. 1277–1279, 2006.

63. Sharma, V., M. Dhayal, Govind, S. M. Shivaprasad, and S. C. Jain, "Surface characterization of plasma-treated and PEG-grafted PDMS for micro fluidic applications," *Vacuum*, Vol. 81, no. 9, pp. 1094–1100, 2007.

64. Dowling, D. P., I. S. Miller, M. Ardhaoui, and W. M. Gallagher, "Effect of surface wettability and topography on the adhesion of osteosarcoma cells on plasma-modified polystyrene," *Journal of Biomaterials Applications*, Vol. 26, no. 3, pp. 327–347, 2011.

65. Mahdavi, M., M. B. Ahmad, M. J. Haron, F. Namvar, B. Nadi, M. Z. Ab Rahman, and J. Amin, "Synthesis, surface modification and characterisation of biocompatible magnetic iron oxide nanoparticles for biomedical applications," *Molecules*, Vol. 18, no. 7, pp. 7533–7548, 2013.

66. Kandpal, N., N. Sah, R. Loshali, and J. Prasad, "Co-precipitation method of synthesis and characterization of iron oxide nanoparticles," *Journal of Scientific & Industrial Research*, Vol. 73, no. February, pp. 87–90, 2014.

67. Lee, J. H., Q. Lu, J. Y. Lee, and H. J. Choi, "Polymer-magnetic composite particles of Fe 3 O 4 /poly(o-anisidine) and their suspension characteristics under applied magnetic fields," *Polymers*, Vol. 11, no. 2, pp. 12–14, 2019.

68. Kim, J. J., R. K. Singh, S. J. Seo, T. H. Kim, J. H. Kim, E. J. Lee, and H. W. Kim, "Magnetic scaffolds of polycaprolactone with functionalized magnetite nanoparticles: Physicochemical, mechanical, and biological properties effective for bone regeneration," *RSC Advances*, Vol. 4, no. 33, pp. 17325–17336, 2014.

69. Tinku, S., E. Iacob, L. Lorenzelli, and R. Dahiya, "Surface characterization of polydimethylsiloxane: An AFM study," in *2015 XVIII AISEM Annual Conference Surface*, pp. 1–4, 2015.

70. Farrell, M., and S. Beaudoin, "Surface forces and protein adsorption on dextran- and polyethylene glycol-modified polydimethylsiloxane," *Colloids and Surfaces B: Biointerfaces*, Vol. 81, pp. 468–475, 12 2010.

71. Palacios-Pineda, L. M., I. A. Perales-Martinez, L. M. Lozano-Sanchez, O. Martínez-Romero, J. Puente-Córdova, E. Segura-Cárdenas, and A. Elías-Zúñiga, "Experimental investigation of the magnetorheological behavior of PDMS elastomer reinforced with iron micro/nanoparticles," *Polymers*, Vol. 9, p. 696, 12 2017.

72. Sharma, D., W. Jia, F. Long, S. Pati, Q. Chen, Y. Qyang, B. Lee, C. K. Choi, and F. Zhao, "Polydopamine and collagen coated micro-grated polydimethylsiloxane for human mesenchymal stem cell culture," *Bioactive Materials*, Vol. 4, no. February, pp. 142–150, 2019.

73. Meade, A. D., F. M. Lyng, P. Knief, and H. J. Byrne, "Growth substrate induced functional changes elucidated by FTIR and Raman spectroscopy in in-vitro cultured human keratinocytes," *Analytical and Bioanalytical Chemistry*, Vol. 387, no. 5, pp. 1717–1728, 2007.

74. Toworfe, G. K., R. J. Composto, C. S. Adams, I. M. Shapiro, and P. Ducheyne, "Fibronectin adsorption on surface-activated poly(dimethylsiloxane) and its effect on cellular function," *Journal of Biomedical Materials Research - Part A*, Vol. 71, no. 3, pp. 449–461, 2004.

75. Liu, J. C., S. C. Helishorn, and D. A. Tirrell, "Comparative cell response to artificial extracellular matrix proteins containing the RGD and CS5 cell-binding domains," *Biomacromolecules*, Vol. 5, no. 2, pp. 497–504, 2004.

76. Kim, K., D. Dean, A. G. Mikos, and J. P. Fisher, "Effect of initial cell seeding density on early osteogenic signal expression of rat bone marrow stromal cells cultured on cross-linked poly(propylene fumarate) disks," *Biomacromolecules*, Vol. 10, no. 7, pp. 1810–1817, 2009.

77. Ranella, A., M. Barberoglou, S. Bakogianni, C. Fotakis, and E. Stratakis, "Tuning cell adhesion by controlling the roughness and wettability of 3D micro/nano silicon structures," *Acta Biomaterialia*, Vol. 6, no. 7, pp. 2711–2720, 2010.

78. Rosales-Leal, J. I., M. A. Rodríguez-Valverde, G. Mazzaglia, P. J. Ramón-Torregrosa, L. Díaz-Rodríguez, O. García-Martínez, M. Vallecillo-Capilla, C. Ruiz, and M. A. Cabrerizo-Vílchez, "Effect of roughness, wettability and morphology of engineered titanium surfaces on osteoblast-like cell adhesion," *Colloids and Surfaces A: Physicochemical and Engineering Aspects*, Vol. 365, no. 1-3, pp. 222–229, 2010.

79. Yamashita, D., M. Machigashira, M. Miyamoto, H. Takeuchi, K. Noguchi, Y. Izumi, and S. Ban, "Effect of surface roughness on initial responses of osteoblast-like cells on two types of zirconia," *Dental Materials Journal*, Vol. 28, no. 4, pp. 461–470, 2009.

80. Grzesik, W. J., and P. G. Robey, "Bone matrix RGD glycoproteins: Immunolocalization and interaction with human primary osteoblastic bone cells in vitro," *Journal of Bone and Mineral Research*, Vol. 9, pp. 487–496, 12 2009.

81. Yin, C., Y. Zhang, Q. Cai, B. Li, H. Yang, H. Wang, H. Qi, Y. Zhou, and W. Meng, "Effects of the micro-nano surface topography of titanium alloy on the biological responses of osteoblast," *Journal of Biomedical Materials Research - Part A*, Vol. 105, no. 3, pp. 757–769, 2017.

82. De Luca, A. C., M. Zink, A. Weidt, S. G. Mayr, and A. E. Markaki, "Effect of microgrooved surface topography on osteoblast maturation and protein adsorption," *Journal of Biomedical Materials Research - Part A*, Vol. 103, no. 8, pp. 2689–2700, 2015.

83. Sun, Z., S. S. Guo, and R. Fässler, "Integrin-mediated mechanotransduction," *The Journal of Cell Biology*, Vol. 215, pp. 445–456, 11 2016.

84. Wells, R. G., "The role of matrix stiffness in regulating cell behavior," *Hepatology*, Vol. 47, no. 4, pp. 1394–1400, 2008.

85. Zhang, T., S. Lin, X. Shao, Q. Zhang, C. Xue, S. Zhang, Y. Lin, B. Zhu, and X. Cai, "Effect of matrix stiffness on osteoblast functionalization," *Cell Proliferation*, Vol. 50, no. 3, pp. 1–9, 2017.

86. Amano, M., M. Nakayama, and K. Kaibuchi, "Rho-kinase/ROCK: A key regulator of the cytoskeleton and cell polarity," *Cytoskeleton*, Vol. 67, no. 9, pp. 545–554, 2010.

87. Wittkowske, C., G. C. Reilly, D. Lacroix, and C. M. Perrault, "In Vitro Bone Cell Models: Impact of Fluid Shear Stress on Bone Formation," *Frontiers in Bioengineering and Biotechnology*, Vol. 4, no. November, 2016.

88. Rutkovskiy, A., K.-O. Stensløkken, and I. J. Vaage, "Osteoblast Differentiation at a Glance," *Medical Science Monitor Basic Research*, Vol. 22, pp. 95–106, 2016.

89. Orr, A. W., B. P. Helmke, B. R. Blackman, and M. A. Schwartz, "Mechanisms of mechanotransduction," *Developmental Cell*, Vol. 10, no. 1, pp. 11–20, 2006.

90. Stains, J. P., and R. Civitelli, "Cell-cell interactions in regulating osteogenesis and osteoblast function," *Birth Defects Research Part C: Embryo Today: Reviews*, Vol. 75, pp. 72–80, 3 2005.

91. Painter, K. J., "Continuous Models for Cell Migration in Tissues and Applications to Cell Sorting via Differential Chemotaxis," *Bulletin of Mathematical Biology*, Vol. 71, pp. 1117–1147, 7 2009.

92. Zor, T., and Z. Selinger, "Linearization of the Bradford Protein Assay Increases Its sensitivity: Theoretical and Experimental Studies," *Analytical Biochemistry*, Vol. 308, no. 236, pp. 302–308, 1996.